Accepted Manuscript

Journal of the Geological Society

New onshore insights into the role of structural inheritance during Mesozoic opening of the Inner Moray Firth Basin, Scotland

A. Tamas, R.E. Holdsworth, J.R. Underhill, D.M. Tamas, E.D. Dempsey, K. Hardman, A. Bird, D. McCarthy, K.J.W. McCaffrey & D. Selby

DOI: https://doi.org/10.1144/jgs2021-066

To access the most recent version of this article, please click the DOI URL in the line above. When citing this article please include the above DOI.

Received 28 May 2021
Revised 12 September 2021
Accepted 27 September 2021

Supplementary material at https://doi.org/10.6084/m9.figshare.c.5635432

New onshore insights into the role of structural inheritance during Mesozoic opening of the Inner Moray Firth Basin, Scotland

A. Tamas[1], R.E. Holdsworth,[1,2], J.R. Underhill[3], D.M. Tamas[4], E.D. Dempsey[5], K. Hardman[5], A. Bird[5], D. McCarthy[6], K.J.W. McCaffrey[1,2], D. Selby[1,7]

[1]Department of Earth Sciences, Durham University, Durham, UK.

[2]Geospatial Research Ltd, Durham DH1 4EL, UK

[3]Shell Centre for Exploration Geoscience, Institute of GeoEnergy Engineering, Heriot-Watt University, Edinburgh, UK.

[4]Centre for Integrated Geological Studies, Babes-Bolyai University, Cluj-Napoca, Romania

[5]Department of Geology, Hull University, Hull, UK.

[6]British Geological Survey, Edinburgh, UK.

[7]State Key Laboratory of Geological Processes and Mineral Resources, School of Earth Resources, China University of Geosciences, Wuhan, Hubei Province 430074, China

Abstract

The Inner Moray Firth Basin (IMFB) forms the western arm of the North Sea trilete rift system that initiated mainly during the Late Jurassic-Early Cretaceous with the widespread development of major NE-SW-trending dip-slip growth faults. The IMFB is superimposed over the southern part of the older Devonian Orcadian Basin. The potential influence of older rift-related faults on the kinematics of later Mesozoic basin opening has received little attention, partly due to the poor resolution of offshore seismic reflection data at depth. New field observations augmented by drone photography and photogrammetry, coupled with U-Pb geochronology have been used to explore the kinematic history of faulting in onshore exposures along the southern IMFB margin. Dip-slip N-S to NNE-SSW-striking Devonian growth faults are recognised that have undergone later dextral reactivation during NNW-SSE extension. The U-Pb calcite dating of a sample from the syn-kinematic calcite veins

associated with this later episode shows that the age of fault reactivation is 130.99 ± 4.60 Ma (Hauterivian). The recognition of dextral-oblique Early Cretaceous reactivation of faults related to the underlying and older Orcadian Basin highlights the importance of structural inheritance in controlling basin- to sub-basin-scale architectures and how this influences the kinematics of IMFB rifting.

[end]

Key words: Inner Moray Firth Basin, Orcadian Basin, structural inheritance, reactivation, U-Pb calcite geochronology

Many sedimentary basins worldwide are superimposed partially or completely over the sites of older, pre-existing basins, e.g. Colorado Basin (Lovecchio et al. 2018); East African Rift (Macgregor 2015; Ragon et al. 2018); the Gulf of Aden (Fournier et al. 2004); the Northeast Atlantic margin (Hansen et al. 2012; Henstra et al. 2019); East Greenland rift system (Rotevatn et al. 2018), the North Sea Rift (e.g. Tomasso et al. 2008) and the West Orkney Basin (Wilson et al. 2010). The role of inherited structures is commonly difficult to constrain in such settings due to the limited resolution of seismic data in offshore regions, whilst onshore areas may be limited by restricted surface exposure and lack of evidence to constrain the absolute age of fault movements. Yet, a better understanding of how earlier-formed faults localise deformation and interact during rifting can give key insights into basin development and potentially reduce sub-surface uncertainties. One potentially useful approach is to focus on well exposed coastal outcrops where structures imaged offshore can be traced directly or indirectly onshore. In many cases, individual faulting episodes will be associated with syn-tectonic mineral fills - such as calcite or base metal sulphides

- which can then be dated using radiometric methods (e.g., U-Pb calcite) to constrain the age of specific faulting episodes (e.g. see approach used by Dichiarante et al. 2016; Roberts et al. 2020). In particular in-situ LA-ICP-MS U-Pb calcite dating has become highly popular in recent years. Calcite can incorporate uranium upon its formation, making it a potentially suitable chronometer for U–Pb and U–Th geochronology allowing it to be used to provide direct timing constraints for a broad range of geoscience applications, including the timing of vein formation and crustal fluid flow (Roberts et al. 2020; Kylander-Clark 2020). Using in-situ LA-ICP-MS allows the targeting of specific microstructural features of carbonate-bearing fault rocks (Hoareau et al. 2020), giving a much more rigorous approach to calcite U-Pb dating of complex geological regions with multiple tectonic or fluid flow events.

This paper focuses on the nature, age and regional significance of faulting and fracturing present in the onshore Devonian succession of the southern IMFB and Orcadian Basin (Fig. 1a-c). New detailed field observations in the Turriff Sub-basin (Fig. 1c) coupled with U-Pb dating of syn-kinematic calcite mineralisation are used to document and characterise the kinematic history of faulting. The latter is utilised to explore the role that inherited Devonian structures played in basin development during subsequent (Mesozoic and Cenozoic) deformation. These findings reveal hitherto unrecognised evidence for interactions between younger rifting episodes and pre-existing sub-seismic-scale Devonian structures, providing a potential new structural template for interpretation of the subsurface basin architecture in the offshore IMFB and elsewhere.

Geological overview

The IMFB is a superimposed basin founded on Precambrian to Caledonian metamorphic basement and post-orogenic Devonian-Carboniferous sedimentary

rocks related to the Orcadian Basin. From Permian until Cretaceous times it forms the western arm of the intra-continental North Sea trilete rift system (McQuillin et al. 1982; Frostick et al. 1988; Roberts et al. 1990; Andrews et al. 1990; Underhill 1991; Thomson and Underhill 1993) that was created following a period of transient thermal doming in the mid-Jurassic (Underhill and Partington 1993). The basin is bounded by major faults, including the Banff Fault to the south, the Helmsdale and Great Glen faults to the northwest, and the Wick Fault to the north (Fig. 1b). The IMFB transitions eastwards into the Outer Moray Firth Basin, which links into the Central and Viking grabens in the central part of the North Sea. The IMFB is widely believed to record important episodes of Late Cretaceous- to Cenozoic-age regional uplift and faulting, including dextral reactivation of the Great Glen and sinistral reactivation of the Helmsdale faults (e.g. Underhill 1991; Thomson and Underhill 1993; Le Breton et al. 2013).

The Mesozoic IMFB overlies the Devonian successions occupying the southern part of the Orcadian Basin (Fig. 1b; Johnstone and Mykura 1989; Friend et al. 2000). The earlier basin is a predominantly fluvial and lacustrine, intracratonic feature belonging to a much larger system of Devonian-Carboniferous basins that extends northwards into Shetland, western Norway, and eastern Greenland (Seranne 1992; Duncan and Buxton 1995; Woodcock and Strachan 2012).

The potential influence of older structures related to the Orcadian Basin on the geometry and kinematics of later IMFB opening has to date received little attention, partly due to the poor resolution of offshore seismic reflection data at depth, or sparse well data. It has been speculatively suggested, based on offshore data, that Orcadian Basin structures may have been reactivated in the IMFB (e.g.

Norton et al.1987; Coward et al. 1989), but little compelling evidence for this inheritance has yet emerged and its potential importance remains uncertain.

Stratigraphic and structural setting

Orcadian Basin

The Lower Devonian, basal part of the Orcadian Basin fill is represented by syn-rift alluvial fan and fluvial–lacustrine deposits. These units are mostly restricted to the western onshore-offshore parts of the IMFB (Rogers et al. 1989) and some areas of Caithness (NIREX 1994a), with excellent exposures of limited extent also seen in the Turriff Sub-basin on the southern coast at Pennan-New Aberdour (Figs 1b, c and 2; e.g. Coward et al. 1989). Here, the Lower Devonian rocks unconformably overlie or are faulted against Neoproterozoic basement of the Dalradian Supergroup. They are thought to have been deposited in a series of small fault-bounded graben of limited extent (e.g. Friend et al. 2000). These strata are unconformably overlain by Middle Devonian syn-rift alluvial, fluvial, lacustrine and locally marine sequences. Rocks of this age dominate the onshore sequences exposed in Caithness, Orkney and Shetland (Marshall and Hewett 2003). They are, in turn, overlain by Upper Devonian post-rift fluvial and aeolian sedimentary rocks (Friend et al. 2000). Younger Carboniferous fills conformably overlie Devonian strata and are restricted to presently offshore regions of the Orcadian Basin. They comprise sandstones, conglomerates, and sparse claystones and siltstones interpreted as part of a regional fluvial depositional setting (e.g. Marshall and Hewett 2003).

The tectonic origin of the Orcadian and nearby West Orkney basins (Fig. 1b) has long been a matter of some controversy and debate. Interpretation of deep and shallow commercial seismic reflection profiles north of Scotland suggested that the

West Orkney Basin comprises a series of half-grabens bounded by easterly dipping normal faults (e.g. Brewer and Smythe 1984; Coward and Enfield 1987). Earlier interpretations (e.g. McClay et al. 1986; Enfield and Coward 1987) postulated that much of the basin fill here was Devonian and that the Orcadian - West Orkney basins formed due to extensional collapse of the Caledonian orogen. More recent studies have cast doubt on these models, showing that the fill of the West Orkney Basin is mostly Permo-Triassic (e.g. Stoker et al. 1993) and that there is only limited onshore evidence for basement reactivation along the N coast of Scotland (e.g. Roberts and Holdsworth 1999; Wilson et al. 2010). Rifting in northern Scotland during the Devonian is now considered to be related to regional sinistral transtension during left-lateral shear along the Great Glen–Walls Boundary fault system (Seranne 1992; Dewey and Strachan 2003; Watts et al. 2007). However, Norton et al. (1987) argued against the dominance of strike-slip related development of the Orcadian basin and proposed a dip-slip evolution during NW-SE extension, and used the Turriff Sub-basin as one of their case studies to support their interpretation.

The Orcadian Basin later experienced a Late Carboniferous-Early Permian inversion event, thought to be related to dextral strike-slip movements along the Great Glen-Walls Boundary fault system (e.g. Coward et al. 1989; Seranne 1992; Watts et al. 2007; Wilson et al. 2010; Dichiarante et al. 2020). This led to regional-scale N-S folding and reverse reactivation of pre-existing Devonian graben-bounding faults from the Scottish mainland to Shetland (e.g. Underhill and Brodie 1993; Dichiarante et al. 2020; Armitage et al. 2021). In Caithness these structures are then everywhere crosscut by younger, predominantly normal faults formed during a later NW-SE rifting event (Wilson et al. 2010; Dichiarante et al. 2020). Dichiarante et al. (2016) used Re-Os geochronology to date base metal sulphides in syn-tectonic

normal to transtensional fault infills and veins in Devonian rocks of the Dounreay area. These yielded a mid-Permian (267.5 ± 3.4 [3.5] Ma) age of faulting, which Dichiarante et al. (2016, 2020) argued was related to the development of the offshore West Orkney Basin located just the northwest. Therefore, they viewed the latter basin as being younger, geographically separate and partially superimposed over the western flanks of the older Orcadian basin and its associated Devonian fills.

The Inner Moray Firth Basin

The stratigraphy of the IMFB (Fig. 2) is known from both surface (e.g. Hurst 1981; Pickering 1984; Frostick et al. 1988) and sub-surface studies (e.g. Andrews et al. 1990; Roberts et al. 1990). The outcrops in onshore regions to the north and south are dominated by Precambrian basement rocks and Silurian-Devonian Caledonian intrusions that are unconformably overlain by Palaeozoic (mainly Devonian, with lesser amounts of Permian strata) cover sequences (e.g. Johnstone and Mykura 1989; Stephenson and Gould, 1995). Mesozoic strata (Triassic to Jurassic) have a limited extent onshore and occur almost entirely along costal margins (Fig. 1b; e.g. Trewin and Hurst 2009; Trewin 1987). Offshore, the sub-crop of the basin is dominated by Mesozoic-Cenozoic sedimentary rocks (Fig. 1b; e.g. Andrews et al. 1990; BGS 1995).

The IMFB is traditionally viewed as having opened during superimposed Permo-Triassic and Late Jurassic-Early Cretaceous rifting episodes, followed by episodes of subsidence, uplift and fault reactivation during the Late Cretaceous to Cenozoic (e.g. McQuillin et al. 1982; Underhill 1991; Thomson and Underhill 1993). The importance of Permo-Triassic rifting - which is widely recognised in other parts of the North Sea (e.g. Steel and Ryseth 1990; Bell et al. 2014; Fazlikhani et al. 2020)

- is debatable in the IMFB due to poor resolution of seismic reflection data at depths where Permo-Triassic strata are imaged, sparse well data, and limited onshore exposures. Early models suggested that during the Permo-Triassic, the basin evolved as a simple half-graben tilted against the Great Glen and Helmsdale faults (Frostick et al.1988). Other authors favoured a transtensional origin for the IMFB (e.g. McQuillin et al. 1982; Bird et al. 1987; Roberts et al. 1990). Such models typically assumed that the Great Glen Fault formed the main controlling structure and suggested that the basin opened as a result of dextral movements along this structure during NE-SW extension. McQuillin et al. (1982) estimated ca. 8 km of displacement along the Great Glen Fault which then generated 5-6 km of extension between the Wick and Banff boundary faults.

The transtensional models and the role of the Great Glen Fault during basin opening were challenged based on findings in a series of later studies (e.g. Underhill 1991; Thomson and Underhill 1993; Underhill and Brodie 1993). Largely based on detailed interpretation of seismic profiles and construction of thickness maps between key stratigraphic intervals, Underhill (1991) proposed a new model for the evolution of the IMFB. He suggested that, after a long period of thermal subsidence during the Triassic to Middle Jurassic, the basin opened mainly during the Late Jurassic under an orthogonal extensional regime. The main displacements are interpreted to lie along the Helmsdale Fault, as the synkinematic sequence thickens without change across the Great Glen Fault, and towards the Helmsdale Fault. This indicates that the former structure was inactive during the Late Jurassic. The widespread recognition of Jurassic-age syn-tectonic fault scarp breccias (locally termed the Boulder Beds) in the hanging-wall of the Helmsdale Fault onshore, along the north coast of the IMFB, further supports fault activity at this time during basin

opening (e.g. Trewin and Hurst 2009; McArthur et al. 2013). In contrast to the previously suggested oblique- or strike-slip deformation under a NE-SW stress regime (e.g. McQuillin et al. 1982; Andrews et al. 1990), Underhill (1991) proposed an orthogonal NW-SE to NNW-SSE extension direction across the Wick and Helmsdale faults. This is similar to the regime suggested by Davies et al. (2001) for the wider North Sea region during the Oxfordian and early Kimmeridgian, following a shift from E–W extension during the Bathonian and Callovian which generated N-S-trending structures in the Central Graben. The rifting in both the IMFB and wider North Sea is considered to be characterised by multiple stages of faulting separated by periods of near tectonic quiescence and is now generally thought to continue until the Early Cretaceous (e.g. Andrews et al. 1990; Davies et al. 2001; Zanella et al. 2003).

Limited information exists in the IMFB about a more detailed structural evolution and timing of fault activity, and it is also uncertain as to when rifting ended during the Early Cretaceous. Underhill (1991) suggested rifting up to the Berriasian followed by (post Berriasian) onlap and regional subsidence in an underfilled basin. Davies et al. (2001) consider that during the Kimmeridgian and Volgian, mainly NW-SE-trending faults developed under a NE-SW rifting direction, and that this extension ceased in the Berriasian. Andrews et al. (1990) imply that rifting continued until later in the Lower Cretaceous based on the preservation of thick (1.6 km) Valanginian to Albian syn-rift deposits in the hangingwall of the Little Halibut Fault (Fig. 1a). Roberts et al. (1990) identified the first reflector onlapping the syn-rift strata in the western part of the IMFB as near top Hauterivian. Argent et al. (2002) suggest the Smith Bank fault was active until the Hauterivian. It is generally agreed, however, that

following the cessation of rifting, the basin then experienced a period of thermal subsidence during the Late Cretaceous (e.g. Andrews et al. 1990, Underhill 1991).

From the early Cenozoic to the present day, the IMFB is thought to have experienced episodes of uplift with regional erosion and eastward tilting, with some major faults undergoing reactivation (e.g. Underhill 1991; Argent et al. 2002). These events have been variously related to the uplift caused by the regional development of the early Iceland mantle plume, the far field effects of the Alpine Orogeny, or to plate readjustment during the opening of the North Atlantic rift (see Le Breton et al. 2013 and references therein). The Great Glen Fault is believed to be the major controlling structure in the basin at this time (Underhill 1991). Offshore, seismic reflection profiles show evidence for the development of strike-slip related deformation patterns including flower structures, folds and offset post-rift reflectors (e.g. Thomson and Underhill, 1993, Underhill and Brodie; 1993; Davies et al. 2001). Onshore evidence of Cenozoic structures supposedly includes the development of large-scale folds, of about 500m wavelength trending NW-SE, in the hangingwall of Helmsdale fault (Thomson and Underhill 1993; Thomson and Hillis 1995). In addition, minor folds and faults in the Jurassic strata exposed at Black Isle and Easter Ross (Fig. 1b) are considered to be Cenozoic and related to right-lateral slip of the Great Glen Fault (e.g. Underhill and Brodie 1993; Le Breton et al. 2013). The effects of Cenozoic deformation away from Great Glen Fault are less certain.

Turriff Sub-basin

Our study area lies in part of the N-S-trending Turriff Sub-basin (Fig. 1c), one of the largest Devonian outliers in the onshore Central Highlands (e.g. Stephenson and Gould 1995). The basin extends for c. 11 km along the southern coast of the IMFB

from Gamrie Bay at Gardenstown to Dundarg Castle at New Aberdour Bay and extends inland and southwards c. 40km to Fyvie (Fig. 1c). This location was chosen for study firstly due to the relatively good coastal exposures, and secondly because it presents a better opportunity to characterise both the Devonian and Mesozoic deformation patterns that are widely overprinted and obscured on the northern margins of the IMFB due to the effects of later supposedly Cenozoic reactivation along the Great Glen Fault zone (e.g. Le Breton et al. 2013).

The Turriff Sub-basin is a Devonian half-graben, bounded to the W by the Afforsk Fault whilst the eastern side is both faulted and locally unconformable on the Dalradian metamorphic basement (Fig 1c; e.g. Read 1923; Ashcroft and Wilson 1976; Trewin 1987). The stratigraphy, sedimentology and interpretation of depositional environments have been studied in some detail and it is generally agreed that the basin fill consists of both Lower and Middle Devonian rocks, assigned, respectively, to the Crovie and Findon groups (Fig. 2; e.g. Read 1923; Trewin 1987). An angular unconformity, considered the boundary between the two groups, is exceptionally well exposed at Pennan (Fig. 1c; BGS 1987; Trewin 1987; Gunn et al. 2015). The succession, having a total thickness of up to 800 m in the northern part and 1400 m in the southern part of the basin (e.g. Gunn et al. 2015), is dominated by breccias and conglomerates, with minor sandstones and mudstones all of which show marked lateral facies variations. Both successions are interpreted to belong to alluvial fan systems with adjacent mudflats and playa lake deposits (e.g. Sweet 1985; Trewin 1987; Trewin et al. 1987). The breccias and conglomerates of the Crovie Group contain granitic and felsitic clasts, while the Findon Group is dominated by clasts derived from the local Dalradian Macduff Slate (Trewin 1987).

The structural style of the Turriff Sub-basin is regarded as complex, especially on the IMFB coast (Ashcroft and Wilson 1976). The bedding is mostly gently westward dipping (e.g. Sweet 1985; Trewin 1987; Gunn et al. 2015), but Read (1923) in his detailed work noted a greater variability of dips. Several fault networks have been recognised based on surface geological mapping (e.g. Read 1923; Sweet 1985; Trewin 1987), gravity data (Ashcroft and Wilson 1976) or interpretation of nearby offshore seismic reflection profiles (e.g. Norton et al. 1987). The dominant fault strikes are predominantly NNE-SSW, parallel to the basin margins (e.g. Ashcroft and Wilson 1976; Sweet 1985; Trewin 1987; Coward et al. 1989). Ashcroft and Wilson (1976) interpreted fault development to have occurred during Devonian rifting based on comparisons with other parts of NE Scotland. Norton et al. (1987) suggested that the Devonian faults were highly arcuate along ESE-WNW, ENE-WNW and N-S trends. They proposed an overall NW-SE extension direction during the Devonian that would require a significant strike-slip component to occur along the segments of these faults which are obliquely oriented to the inferred rifting vector.

A younger set of faults trending ENE-WSW (e.g. Sweet 1985; Trewin 1987) were considered by Ashcroft and Wilson (1976) to have initiated during Permo-Carboniferous times, based on the observation that a dyke swarm interpreted by Buchan (1932) to be of that age has a similar trend across NE Scotland. These authors also noted that this ENE-WSW trend is approximately parallel to the southern margin of the IMFB and suggested that movements along structures with this trend continued into the Mesozoic.

Methods

Fieldwork and stress inversion analyses

The field data described in this study focuses on the Lower and Middle Devonian coastal outcrops of the onshore Turriff Sub-basin (Fig. 1c). Kilometre-long exposures of Crovie and Findon groups (Read 1923; Trewin 1987) in the central and eastern part of the sub-basin show representative sequences of events and variety of brittle deformation structures. The outcrops are referred to as the Pennan and New Aberdour localities (Fig. 1c) here based on their proximity to nearby villages.

In-situ detailed field observations and measurements of bedding, faults, fractures, folds, fault rocks and associated mineralisation were recorded. Where accessible, the structural measurements were taken using both a Suunto geological compass/clinometer and the FieldMove™ digital mapping application on an Apple iPad™ (6th Generation). At each locality studied, the relative ages of structures were carefully assessed using cross-cutting relationships. The sense of fault movement was determined based on the presence of offset stratigraphic markers, kinematic indicators such as slickenlines, in addition to shear sense criteria such as asymmetric, en-echelon arrays of Riedel or tensile veins (e.g. Petit 1987).

Structural data processing and visualisation were carried out using Stereonet 10 (Allmendinger et al. 2012; Cardozo and Allmendinger 2013). The measurements were graphically represented using both rose diagram plots of azimuth distributions (at 10° sector angles) and equal area stereonets, lower hemisphere projection using poles to planes where appropriate. The contouring was calculated after Kamb (Kamb 1959) at 2 and 3 sigma standard deviation above a random population.

Fault-slip slickenline data were collected in-situ from exposed fault surfaces in order to perform a palaeostress inversion. This analysis assumes that slip on a fault surface occurs in the direction of the maximum resolved shear stress (Wallace 1951;

Bott 1959). Numerous methods have been developed to invert fault kinematic data and derive palaeostress (e.g. Spang 1972; Michael 1984; Angelier 1984,1990; Mostafa 2005) by obtaining the orientation of the three principle stress axes (σ_1, σ_2, and σ_3 which are the maximum, the intermediate, and the minimum principal stresses, respectively) and the stress ratio (R) which is defined as $(\sigma_1 - \sigma_2)/(\sigma_2 - \sigma_3)$, also called the reduced stress tensor. In this study, the fault data were analysed using the Angelier (1990)'s direct inversion method (INVD) implemented using the SG2PS software (Sasvári and Baharev 2014). This method estimates the reduced stress tensor and the shear stress magnitudes from the fault-slip data (Angelier 1990). The program also graphically computes the stress regime based on the stress index (R') (Delvaux et al. 1997). The stress index is based on the identity of the vertical stress axes and the stress ratio as follows: radial extension (σ_1 vertical, $0 < R < 0.25$); pure extension (σ_1 vertical, $0.25 < R < 0.75$); transtension (σ_2 vertical, $0.75 < R < 1$ or σ_2 vertical, $1 > R > 0.75$); pure strike-slip (σ_2 vertical, $0.75 > R > 0.25$); transpression (σ_2 vertical, $0.25 > R > 0$ or σ_3 vertical, $0 < R < 0.25$); pure compression (σ_3, vertical, $0.25 < R < 0.75$); and radial compression (σ_3 vertical, $0.75 < R < I$). The stress index is expressed numerically as continuous values between 0 and 3, where values ranging from 0 to 1 are defined for extensional stress regimes ($R' = R$, σ_1 is vertical), 1 to 2 for strike-slip stress regimes ($R' = 2 - R$, σ_2 is vertical), and from 2 to 3 for compressional stress regimes ($R' = 2 + R$, σ_3 is vertical) (for more details see Delvaux et al. 1997).

Photogrammetry

Photogrammetry, especially UAV-based photogrammetry, is a valuable and increasingly used technique as it allows a visual assessment of the spatial distribution of structures across a wide range of scales (cm to km) and gives greater

access given to otherwise inaccessible parts of the outcrop in cliffs. It also allows the routine extraction of structural observations and data from 3D digital outcrop models (DOM) (e.g. McCaffrey et al. 2005; Weismüller et al. 2019; Tamas et al. 2021). In our case, the acquisition of UAV photography was made using a DJI Mavic Air drone, which has a digital camera with a 12-megapixel image sensor.

For horizontal exposures, we used a pre-set automated flight path and data acquisition process. This was achieved with the use of Pix4Dcapture software, used with an Apple iPad (6^{th} generation). The acquisition parameters were a front overlap of 80% and a side overlap of 70%, and a 70° camera angle. The altitude of acquisition varied between a few centimetres to 50 meters. For the vertical or steeply inclined cliff exposures, we used a manual flight path and image acquisition process. The camera was oriented orthogonal to the exposure and we tried to achieve a similar level of overlap to the automated acquisition.

For the creation of the DOM, DEM (digital elevation models) and orthorectified models, we used Agisoft Metashape Professional™ (v.1.6.2). The process of constructing the models involves a series of steps to create an accurate photograph alignment which then leads to the development of a sparse point cloud, followed by the creation of a dense point cloud, mesh, and texture. The 3D textured meshes (DOM), together with the dense point cloud data, were imported into Virtual Reality Geological Studio (VRGS v.2.52) software (Hodgetts et al. 2007) to allow structural interpretation and extraction of structural orientation data. These included bedding, fault and fracture orientations. Where presented together with structural data collected by hand, these readings are shown in a different colour on stereoplots. In order to reduce uncertainties regarding the positioning and orientation of the 3D outcrops and orthomosaics, several orientation measurements were ground-truthed.

The orthomosaic orientation has also been cross-checked with satellite imagery data. Lineament orientation analysis was performed using FracPaQ (Healy et al. 2017), a MATLAB-based toolbox.

Microscopy and U-Pb geochronology

Structurally-oriented samples of calcite mineral fills associated with specific fault zones recognised during fieldwork were collected for microscopic and geochronological analysis. U-Pb analysis of four calcite fracture fills was undertaken at the University of Hull using in-situ laser ablation inductively coupled mass spectrometry (LA-ICP-MS). Ablation was carried out using an Applied Spectra, RESOlution-SE 193nm laser with a Laurin Technic S155 two volume cell, laser wavelength of 193 nm, pulse width of 5 ns, fluency of 5 j/cm^2, repetition rate of 10 Hz, ablation time of 30 s, 100 micron spot size. Helium and N_2 were used in the cell with Ar acting as the main carrier gas. Isotopic analyses were carried out using an Agillent 8800 ICP-MS with an RF power of 1170 W, nebuliser gas flow of 0.86 l/min with the electron multiplier in counts per second mode. All samples were tested and mapped for uranium content in order to ascertain whether they contain sufficient abundance of ^{238}U in order to yield a Model 1 U-Pb discordia age. Isotopic mapping was carried out on polished chips with a fluency of 5 j/cm^2, on laser energy of 6.4 mJ, square 80 x 80 µm spot size and a scan speed of 20 µm/s with a repetition rate of 10 Hz. All uncertainties were propagated in the Iolite software package following the approach used in Holdsworth et al. (2020). The Iolite software uses the reference standard analyses to estimate the propagated analytical uncertainty. This is done by individually removing each analysis and treating it as an unknown which results in a population of pseudo-secondary standards. It does not address any potential

sources of bias (e.g., nonmatrix matched standards, or measurement biases between zircon standards). Uncertainties are further propagated through the addition of the standard reference material uncertainties in quadrature. The U-Pb data is presented on Tera-Wasserburg plot and a model 1 age calculated (with age and $Pb_{initial}$ uncertainties quoted as 2σ) using IsoplotR (Vermeesch 2018).

Only one sample (S02) contained sufficient ^{238}U abundance (and low common lead values) in order to yield an accurate and precise date. A further sample (S01) was also analysed at the BGS Isotope Geosciences Laboratory, but did not contain sufficient amounts of ^{238}U compared to common lead to yield suitable U/Pb ratios to produce a geologically meaningful date. Analytical protocols and analysed sample details are provided in the Supplementary Materials.

Thin sections were studied and photographed using an optical transmitted light microscope to ascertain the relative age of the mineral fills, any fault-related displacements and deformation. A key requirement here was to demonstrate that the growth of calcite could be shown to be synchronous with fault displacements recognised during fieldwork. Thin sections from three representative samples from New Aberdour (S01-S03) are used in this paper to illustrate our findings.

Results

Fieldwork

Pennan [NJ 845 654]

The village of Pennan lies in a central location along the coastal outcrop of the Turriff Sub-basin Devonian fill (Fig. 1c). The exposure studied here is about 1 km long and extends from Millshore [NJ 84059 65813] to Pennan Harbour [NJ 84716 65551] (Fig.

3a). The exposure comprises limited wavecut platforms and very good coastal cliff exposures 10 to 25 m high, that are fully accessible at intermediate and low tides. The rocks exposed belong to both the Crovie and Findon groups (Fig. 2; Read 1923; Trewin 1987). Both sequences here are predominantly composed of red conglomerates, breccias and sandstones and are interpreted to have formed in alluvial fan systems (e.g. Trewin 1987). The Findon Group is generally coarser grained, dominated by m-thick breccias with angular and subangular cm- to dm-scale fragments of Dalradian basement (Macduff Slates). Only a few cm-thick layers of medium-course red-coloured sandstone, usually lensoid (e.g. Fig 4b, c) can be observed, while in the older Crovie Group, red-coloured sandstones are better developed. The sandstone beds here can be more than a meter thick, but are more usually 10 to 50 cm in thickness (e.g. Figs 4b and 5). In the cliff exposure close to Pennan harbour (Figs 3b and 5c), they form a sandstone-dominated sequence with a vertical extent of at least 25 m. East of Millshore, below the Nethermill Cottages [NJ 84255 65724], an angular unconformity between the Crovie and Findon groups is beautifully exposed in coastal cliff and foreshore exposures (Fig. 4; see also Trewin 1987; Norton et al. 1987). This location is traditionally considered to be the only place within the Orcadian Basin where an angular unconformity between the Lower and Middle Devonian sequences can be directly observed (e.g. Norton et al. 1987).

In both the Crovie and Findon groups, bedding orientations are quite variable, dipping gently to steeply (~15° to 70°) usually towards the E or W, and more locally in other directions (Fig. 3c). Close to Millshore, the bedding dips mainly ~30° to 50° E/ESE (Fig. 3b). Walking east, in the cliffs below Nethermill Cottages, the dips steepen up to 70° and are usually inclined towards the west, whilst about 100-150 m

from the cliffs to the north in the wavecut platform, the dips are shallower and are generally towards the NE (Fig. 3b). The beds are also more gently dipping NW on the eastern side of Pennan Bay, close to the harbour (Fig. 3b).

The Crovie and Findon groups are crosscut by numerous, commonly closely-spaced (decimetre to metre separation) faults, fractures or fracture corridors and veins (e.g. Figs 4 to 6). Fault displacement histories are complex, but most faults show a significant component of normal movement based on offsets of bedding markers. The main set of faults and fractures have two preferred orientations. The dominant set trend broadly N-S (~30°scatter) dipping both E and W, while a second set trend NE-SW (~60° scatter) (Fig. 3d). The normal fault planes typically have high to sub-vertical dips (60 to 88º), but less common, shallowly-dipping faults of about 20°- 40° are also encountered locally (Fig. 3d).

In the cliffs below the Nethermill Cottages, the angular unconformity between the Lower and Middle Devonian is spectacularly exposed in an outcrop 15 m wide and 20 m high, forming a local half-graben tilted towards the E (Fig. 4a). The sequence is affected by a series of decimetre- to metre-spaced normal offset faults (e.g. Fig. 4b and c). The amount of offset along individual faults is usually difficult to quantify due to the lack of stratigraphic markers, but where it can be observed, faults show dip-slip displacements ranging from a few centimetres (e.g. Fig. 5a) up to several metres. Clear thickening of the strata can be observed in the hangingwalls of faulted units both below and above the unconformity, illustrating the persistent and syn-kinematic nature of growth faulting during deposition of both the Crovie and Findon group strata (Figs 4 and 5a). While some growth faults do not pass up into the younger Middle Devonian succession, others clearly do continue and also show growth thickening of beds into fault hangingwalls within the younger stratigraphy

(Fig. 4). The faulted blocks show locally significant amounts of rotation (~40º), and this has contributed to the markedly angular nature of the unconformity developed between what are considered to be Lower and Middle Devonian strata (e.g. BGS 1987; Trewin 1987). The prominent low angle fault (highlighted in bright red) at the base of the outcrop in Figure 4 shows growth strata both in the hangingwall (Fig. 4b and c) and (apparently) in the footwall (Fig. 5a). This aspect can be explained by subsequent cross-cutting faulting and block rotation (Fig. 5c).

Close to Pennan harbour, a previously mapped (e.g. Trewin 1987; BGS 1995) major N-S-trending fault juxtaposes Middle Devonian hangingwall strata to the west against a Lower Devonian footwall to the east (Fig. 3b). The fault core is not exposed, but about 70 m east in the footwall of the fault, a ~10 m wide fault-parallel deformation zone is exposed. It is characterised by multiple decimetre-spaced faults and fractures (Fig. 5d). Most are shallow to steeply dipping (~10-85º), NW-SE-trending structures. Here, the low angle planes appear to be more shallowly-dipping segments of a series of curved or listric geometry faults, which have higher dips in the upper part, decreasing to (near) horizontal down dip (e.g. Fig. 5d).

The fault rocks and mineral fills associated with the brittle structures identified at Pennan can be divided in two main types. The first group comprises fault zones characterised by sharply-defined, clean breaks (e.g. Figs 5a, d, e), sometimes associated with dm-thick fault breccia infilling dilatant jogs, and dark red or green gouges. We refer to these as '*non-mineralised faults'*. The other fault group is marked by the development of calcite-cemented breccias (Fig. 6a, b), calcite tensile veins (Fig. 6d) and calcite slickenfibres developed along shear plane surfaces. We refer to these as '*calcite-mineralised faults'*.

The non-mineralised faults predominantly trend N-S to NNE-SSW and NW-SE (Fig. 5b). Although kinematic indicators are uncommon, slickenline lineations and grooves are sometimes preserved, especially in finer-grained units of the Crovie Group (e.g. Fig. 5d and e). The fault panels of N-S- to NNE-SSW-trending structures typically show dip-slip to sinistral-oblique kinematics (~50° to 85° pitch), while the NW-SE-trending faults are usually dip-slip (80-90° pitch, e.g. Fig. 5d and e).

The calcite-mineralised faults and veins predominantly trend NE-SW, but N-S- to NNE-SSW- or NW-SE-trending faults are also present (Fig. 6c). Calcite mineralisation is mainly seen in patches, cementing the breccia in fault zones (Fig. 6a, b) or in adjacent wall rocks forming tensile veins of less than 1mm to several cm thick (Fig. 6d). The NE-SW trend is well represented by tensile veins observed in close proximity to N-S-trending faults (Fig. 6d). A key feature of the calcite mineralised faults is that, in contrast to the non-mineralised structures, the N-S- to NNE-SSW-trending faults show dextral to oblique-dextral/normal kinematics. This is indicated by both slickenlines identified on the fault panels and also by asymmetrically associated tensile veins arranged in en-echelon arrays. Figure 6d shows an example of oblique dextral slip associated with one of the major N-S-trending, steeply dipping faults (80/270) which can be traced in both the cliffs and wave-cut platform. The fault is associated with en-echelon, calcite-mineralised tensile veins trending NE-SW (Fig. 6d.) suggesting a component of dextral slip during NNE-SSW extension (Fig. 6d inset).

New Aberdour [NJ 884 633]

The village of New Aberdour lies on the coast about 7 km east of Pennan. The area is located close to the eastern margin of the Turriff Sub-basin (Fig. 1c). The

investigated exposures extend about 1.5 km along the shoreline of New Aberdour Bay [NJ 885 646]. A flat-lying wave-cut platform 150-200 m wide which is accessible at low tide is present on the west side of the bay (e.g. Fig. 8), while towards the east, both flat-lying platforms and cliffs up to 25 m high are exposed (Fig. 12c).

The exposed Lower Devonian rocks belong to the Crovie Group (e.g. Sweet, 1985; Fig. 7b). On the easternmost side of the bay, the succession unconformably overlies Dalradian basement rocks (Fig. 2b) and comprises metre-thick beds of light red, poorly-sorted breccias with angular/sub-angular clasts of Dalradian basement rocks (mainly andalusite and biotite schist), interpreted to have formed as debris-flow deposits laid down in alluvial fan systems (lithology 6, Fig. 7b; e.g. Sweet 1985; Trewin et al. 1987). The succession continues to the west as medium-grained fluviatile sandstones which are conglomeratic at the base and preserve trough cross bedding locally (lithology 5, Fig. 7b). Based on paleocurrent data, Sweet (1985) suggested that the sediments gradually filled a NNE-SSW-trending palaeo-valley. This sequence is overlain by a meter-thick bedded conglomeratic sequence (lithology 4, Fig. 7b) that becomes thinner-bedded and dominated by sandstones (lithology 3) representing proximal and distal alluvial fan environments, respectively (Sweet 1985). This, in turn, passes upwards into a sequence of cm-thick, fine-grained sandstones, laminated red and green mudstones and limestones (lithology 1 and 2, Fig. 7b). They have been interpreted as alluvial plain/playa lake deposits (e.g. Sweet 1985; Trewin et al. 1987).

Overall, the beds are typically sub-horizontal to gently dipping (02° to 30°) to the WNW but, as seen at Pennan, steeper dips (up to 55°) and a variety of dip directions are encountered locally (Fig. 7b and c). The sequence is crosscut by numerous faults, fractures and veins of variable orientations (Figs 7b-d). These

display components of normal offset along faults where this can be determined from offsets of stratal marker horizons.

A large (50,000 m^2) high resolution orthorectified image (Fig. 8a) and DEM (Fig. 8b) model obtained from UAV photography was acquired from the western side of the bay and enabled a lineament analysis to be performed that revealed the dominant structural trends. The interpretation was verified with field observations to ensure that the picked lineaments corresponded to faults, fractures and veins. 102 lineaments of more than ~10 m length were interpreted within the entire area of the model (Fig. 8c), while 328 lineaments of less than 10 m were measured on a smaller, well-exposed area of about 225 m^2 (Fig. 8d). At larger scales, NNW-SSE to NNE-SSW trends dominate, with subordinate NE-SW- and E-W- to SE-NW-trending structures also present (Fig. 8c.). At smaller scales, the ENE-WSW trend (40° scatter) is better represented, but lineaments trending NNW-SSE to NNE-SSW also occur (Fig. 8d).

Similar to the Pennan locality, the faults and fractures imaged and directly measured in the field can be subdivided into non-mineralised and calcite mineralised groups. The non-mineralised faults trend ESE-WNW and N-S to NE-SW (Figs 9a-c). The fault zones are characterised by sharply defined clean breaks (e.g. Fig. 9b), red/green mm- to cm-thick gouges (Fig. 9a) or cm- to dm-thick fault breccias. Kinematic indicators such as slickenline lineations and grooves are sometimes preserved on exposed fault panels (e.g. Figs 9b and 10c). On ESE-WNW-trending faults, the kinematic indicators are rarely visible. Only one fault preserved indications of normal, dextral oblique-slip kinematics. On N-S to NNE-SSW trends slickenlines indicate dip-slip normal (Fig. 10c.) to slightly sinistral normal, oblique-slip displacements (Fig. 9a).

On the western side of New Aberdour Bay, two intersecting NNE-SSW- (Fault I in Fig. 10a) and NW-SE-trending faults (the latter parallel to a mafic dyke margin) juxtapose the Lower Devonian succession in their hangingwalls against the Dalradian basement slates (e.g. Figs 7b and 10a). The NW-SE-trending fault dips steeply towards the NE (dip/dip direction - 75°/320°) and poorly-preserved slickenlines suggest a normal, sinistral oblique-slip shear sense. The mafic dyke is up to 4 m wide and can be traced for about 150 m to the NW, where it becomes poorly exposed. Other similar sub-vertical (dipping >85°E) dykes have been observed locally in the Dalradian basement, but none are seen to cross-cut the Devonian succession. This suggests that the dykes most likely predate the Crovie Group and could be Ordovician as suggested for other mafic and ultramafic intrusions in this area (e.g. Read 1923; Gunn et al. 2015). Further study is needed to better constrain the nature and age of these dykes.

The NW-SE fault separating basement and cover is crosscut by a steeply E-dipping (80°), calcite-mineralised fault trending NNE-SSW (Fault I, Fig. 10a). This fault has been previously interpreted as a major east-side-down normal fault together with other such faults with this trend in the area (Sweet 1985). Although the exposed fault plane does not preserve kinematic indicators, minor structures present in a 10 m wide damage zone around the fault preserve evidence of shear sense. These include a series of mutually cross-cutting ENE-WSW-trending dextral faults (Fig. 11a), NW-SE sinistral faults and E-W tensile fractures. We interpret these structures as R- and R'-shears and T fractures, respectively, suggesting an overall dextral sense of movement along the main NNE-SSW-trending master fault (Fig. 11d). Other minor dextral N-S- to NNE-SSW-trending faults, parallel to the major fault have also been observed (Fig. 11c). All of these recorded minor structures are calcite-

mineralised. Close to Fault I, drag folding of the Devonian bedding and basement foliation is observed, which is also consistent with dextral movement (Fig. 10a). About 60 m east from Fault I, another major, NNE-SSW tending fault steeply dipping to the E (74°/290°) occurs (Fault II, Fig. 10a). On the exposed fault plane, both dip-slip slickenline lineations (Fig. 10c) and a later set of normal-dextral calcite slickenfibres (Fig. 10d) are preserved, the latter suggesting that some fault movements have occurred synchronously with carbonate mineralisation. Thus the NNE-SSW-trending faults preserve evidence for two episodes of movement: an earlier phase of normal dip-slip and a later set of dextral strike-slip synchronous with calcite mineralisation.

Folds are commonly visible in the Devonian strata exposed on the flat-lying platform, both on the west and east side of the bay (e.g. Fig. 10a and 12a-c). They are usually gentle to open structures (interlimb angles of 120-130°) and plunge shallowly (08-23°) towards the NNW (Fig. 7e). Closer to faults, these folds are tighter (interlimb angles as low as 80°; Fig. 12b) and plunge more steeply (~40°) towards the N. Extension fractures in the outer arcs of the fold hinge zones are calcite-mineralised (Fig 10b) suggesting that the folding occurred synchronously with calcite mineralisation and the associated faulting episode. Folds are consistently spatially associated with mappable faults (Figs 10b and 12a). Their orientation relative to these N-S to NNE-SSW faults is consistent with dextral kinematics and they have formed synchronous with carbonate mineralisation. Away from the faults, bedding is more uniformly dipping to the W (Fig. 7b).

Microscopy

Three representative samples of calcite-mineralised fault zones (S01-03) were selected for microstructural analysis. Sample S01 (Fig. 10d) was collected from the calcite slickenfibers associated with the N-S- to NNE-SSW-trending Fault II (Fig. 10a). Samples S02 (Fig. 11b) and S03 (Fig. 10a) are from minor dextral shear fractures associated with Fault I (Fig. 10a). Further details about the samples are also provided in the Supplementary Material.

All samples show very similar microstructural characteristics (Fig. 13a-f) that are typical of shear veins formed synchronous with fault slip (e.g. see Passchier and Trouw 2005 and references therein). A stacked series of fault-parallel panels with sharp bounding surfaces enclose domains of crystalline and/or fibrous calcite (Fig. 13a and b). The shear veins are either linked together, or locally cross-cut by calcite-filled dilational veins that are consistently oriented sub-parallel to trails of wall rock and fluid inclusions that are best preserved in the fibrous domains (Fig. 13c). The preservation of such inclusion trails is consistent with crack-seal behaviour (Ramsay 1980) and the asymmetry of these trails, the dilational jogs and the fibre obliquity relative to the local fault planes is everywhere consistent with dextral displacements (Fig. 13a, b, d and e). Obliquely-oriented tensile calcite veins in sample S02 are closely associated with small gouge-bearing faults in the wall rocks (Fig. 13d and e) which also locally preserve sub-millimetre-spaced Reidel shears consistent with dextral shear (Fig. 13f). Collectively, these textural relationships indicate that calcite mineralisation and local right-lateral displacements along N-S- to NNE-SSW-trending faults are contemporaneous.

U-Pb geochronology

The ^{238}U and ^{206}Pb concentrations were analysed in five calcite-bearing samples collected in the field (e.g. Fig. 14a). Samples shown to have approximate concentrations of ^{238}U less than 1 ppb were not analysed any further (three samples; see Supplementary Material), whilst samples with concentrations greater than 1 ppb were mapped in detail using the methods described previously. This allowed zones of higher ^{238}U concentration to be identified and targeted for dating. Of the two samples analysed, only one - S02 (Figs 11b and 14a) - contained sufficient amounts of ^{238}U (and low enough concentrations of common Pb) to yield an accurate and precise date (note: LA-ICP-MS data for the unsuccessful sample can be found in the Supplementary Material). For sample S02, 197 spots were ablated, with 68 spots omitted due to excess common Pb or poor ablation. The remaining spot data (N = 129) were plotted on a Tera-Wasserberg U-Pb plot using IsoplotR (Vermeesch 2018) which yielded a $^{238}U/^{206}Pb$ Model 1 age of 130.99 ± 4.60 Ma (2σ, $Pb_{initial}$ = 0.696 ± 0.0016, MSWD = 0.37; Fig. 14b). The final age uncertainty is fully propagated with reference material uncertainties added in quadrature. Note that a Model 1 age of 131.06 ± 4.48 Ma (2σ, $Pb_{initial}$ = 0.700 ± 0.0013, MSWD = 0.37) is yielded when the excluded data are also plotted (see Supplementary Material). The primary reference material used was WC-1 which yielded a $^{238}U/^{206}Pb$ Model 1 age of 257.22 ± 5.32 Ma (2σ, $Pb_{initial}$ anchored at 0.85, MSWD = 0.13) which is within uncertainty of the expected 255.4 ± 6.4 Ma age reported by Roberts et al. (2017). NIST612 was used as a secondary reference material which yielded isotopic concentrations (^{204}Pb = 38.40 ± 0.92, ^{206}Pb = 38.48 ± 0.15, ^{207}Pb = 38.49 ± 0.21, ^{208}Pb = 38.49 ± 0.31, ^{232}Th = 37.73 ± 0.14, ^{235}U = 37.34 ± 1.29, ^{238}U = 37.16 ± 0.48) within uncertainty of the certified values for NIST612 (38.57 ppm Pb, 37.79 ppm Th, and 37.38 ppm U); this

was consistently within 2 SE of our long-term reproducibility (see Supplementary Material).

The low MSWD obtained from the dated carbonate vein sample points to a single isotopic population/mineralisation event, despite the isotopic mapping (Fig 14c) of the sample showing the heterogeneous composition of the precipitated material. The analysed carbonate is enriched in ^{238}U in the vicinity of an incorporated sandstone clast possibly suggesting leaching of metals from the host rock. Isotopic mapping also reveals a spatial link between the higher ^{238}U and ^{206}Pb concentrations with ^{24}Mg enrichment of the carbonate, with ^{238}U being particularly enriched at the interface between the high and low ^{24}Mg zones (Fig 14c). Whether this heterogeneity relates to original fluid compositional change or to later alteration/dolomitization is uncertain, although microstructural evidence for later alteration/replacement has not been seen in the samples studied. Heterogeneous ^{24}Mg compositions occur between individual carbonate crystals on the left had side of the map with a more uniform ^{24}Mg enrichment towards the right-hand side of the image which represents the centre of the vein. This suggests that the chemical heterogeneity was a feature of the original carbonate mineralization in the vein, with the Mg (with U and Pb) becoming enriched in the remaining fluid as the vein closed (entraining the wallrock fragment). We therefore tentatively suggest that the chemical variations mapped represent original vein growth processes rather than later alteration meaning that the $^{238}U/^{206}Pb$ age obtained most likely reflects the time of vein formation and faulting rather than a later fluid flow event.

Main fault types and stress inversion analysis

The N-S to NNE-SSW striking normal to slightly sinistral faults are demonstrably syn-sedimentary based on the growth packages in their hangingwalls (Figs 6 and 7a) and are non-mineralised and characterised by clean breaks, fault gouges or breccias. Palaeostress inversion analysis of these non-mineralised fault slip data yield an ENE-WSW extension direction (Fig. 15a). The inversion suggests that the faults developed in a regime of near-horizontal extensional stress (σ_3) with an axis orientated 07°/061° and near-vertical compressive stress (σ_1) with an axis orientated 81°/272° (Fig. 15a).

The N-S to NNE-SSW striking faults also show evidence of dextral movements (e.g. Fig. 6d), while some preserve evidence of both earlier dip-slip and later dextral-oblique extensional displacement (e.g. Figs 10c and d). This dextral slip is everywhere associated with calcite mineralization. A palaeostress inversion performed on these calcite-mineralised faults shows that they formed during NNW-SSE rifting (Fig. 15b.). The faults were developed in a transtensional regime of horizontal extensional stress (σ_3) with an axis orientated 01°/340° and steeply plunging compressive stress (σ_1) with an axis orientated 67°/247°.

Discussion

Timing and kinematics of faulting

Non-mineralised faulting phase

The NNW-SSE to NNE-SSW-striking faults characterised by unmineralized clean breaks, fault gouges or breccias were demonstrably established during the Lower-Middle Devonian rifting based on the preservation of very well-developed growth packages in their hangingwalls (Figs 6 and 7a). Whilst absolute evidence concerning

the age of faulting is not available, it is clear that at least two periods of growth faulting occurred prior to and following the development of the erosional unconformity that separates the supposedly Lower and Middle Devonian sequences. Different fault orientations showing the same fault rock characteristics are interpreted here as being part of the same deformation event. We cannot exclude the possibility that some of the non-mineralised faults are younger, but we have no independent evidence to suggest this. Some could be Permo-Carboniferous structures as suggested by Ashcroft and Wilson (1976), although no faults similar to the Permo-Carboniferous 'Group 2' structures observed in Caithness (as defined by Dichiarante et al. 2020) have been identified in our study area. Those structures are typically N-S-trending reverse faults caused by localised inversion of earlier Devonian structures, and are typically associated with N-S-trending folds.

The non-mineralised faults identified in the present study show normal to slightly sinistral-oblique displacements as suggested by the preservation of fault lineations and grooves on exposed slip surfaces (e.g. Fig. 5d and e). Palaeostress inversion analysis of these fault slip data yields an ENE-WSW extension direction (Fig. 15a). These results differ markedly from the NW-SE extension direction suggested by Norton et al. (1987), but are comparable to the ENE-WSW extension and similar fault kinematics documented elsewhere in the Orcadian Basin (e.g. Dewey and Strachan 2003; Wilson et al. 2010; 'Group 1' structures of Dichiarante et al. 2020).

We consider that our results show that the generally N-S-trending faults in the Tariff Sub-basin are related to ENE-WSW sinistral transtensional development of the Orcadian Basin during Devonian left-lateral shear along the Great Glen–Walls Boundary fault system (Seranne 1992; Dewey and Strachan 2003; Watts et al. 2007;

Wilson et al. 2010). This suggests that the regional model for Devonian basin development widely recognised north of the Great Glen Fault can be extended to the southern limits of the Orcadian Basin in the Central Highlands.

Mineralised faulting phase

The Devonian sedimentary rocks are locally cross-cut by a set of younger faults, veins and folds that are associated with widespread syn-tectonic calcite mineralisation (e.g. slickenfibres, tensile veins, Riedel shear fractures, or calcite-cemented fault rocks). Some pre-existing Devonian structures, especially the NNE-SSW-trending faults, experienced oblique-dextral reactivation during this later deformation (e.g. Fig. 10). Stress inversion analyses performed on the calcite mineralised faults show that they formed during NNW-SSE transtensional deformation (Fig. 15b). NNW-plunging folds are locally developed in proximity to faults, and show calcite mineralised outer arc extension fractures (Fig. 10b). Although folding seems to be restricted to regions located closer to larger faults, folds developing in an overall transtensional regime are not uncommon (e.g. De Paola et al. 2005; Fossen et al. 2013). Likewise, the oblique-sinistral NW-SW faults are likely to have been developed during the same event as their observed kinematics are consistent with the general NNW-SSE transtensional regime.

The new U-Pb dating of the calcite in sample S02, collected from the minor dextral fault (Fig. 11b) interpreted as a synthetic Riedel to Fault I, yields an Early Cretaceous age of 130.99 ± 4.60 Ma (Hauterivian) (Fig. 14b). The field evidence (Fig. 11b) and microstructural observations (Fig. 13d-f) suggest strongly that fault displacements were contemporaneous with calcite mineralisation. It is therefore

proposed that this age also constrains the timing of the younger phase of faulting recognised in the Devonian rocks along the southern coast of the IMFB.

Implications for the regional-scale deformation history of the IMFB

Permo-Triassic

Dextrally reactivated Devonian structures which suggest NW–SE regional rifting have been identified in the northern part of Caithness, where Re-Os geochronology of syn-tectonic fault-hosted pyrite yielded a Permian age (c. 267 Ma) (Dichiarante et al. 2016). Although somewhat similar in structural style, based on U-Pb dating, the dextral reactivation of the Devonian structures in our study area is much younger (130.99 ± 4.60 Ma). Furthermore, the Caithness veins are widely associated with base metal sulphides in addition to calcite – such minerals have not been observed along the south coast of the IMFB. Although it is at present unclear whether the Permian deformation in Caithness extends southwards to the NW flanks of the IMFB, it does not seem to be clearly preserved in the onshore exposures on the south side of the basin. As suggested by Dichiarante et al. (2016, 2020), the deformation in Caithness is likely related to the opening of the West Orkney Basin, and may not extend south of the Helmsdale Fault. Hence, the question regarding whether there is onshore evidence for Permo-Triassic deformation in the IMFB remains unresolved.

Late Jurassic –Early Cretaceous

Much of the debate about the relative importance of strike-slip vs dip-slip tectonics in the development of the IMFB came prior to the availability of high-resolution 3D seismic data. More recent models, based on subsurface data of this kind, tend to suggest that there is little evidence for the development of syn-rift oblique-slip faults

in the basin (e.g. Davies et al. 2001; Long and Imber 2010; Lapadat et al. 2018). The dextral movement of the Great Glen Fault which generated oblique- or strike-slip faults in the basin are widely considered Cenozoic as they also displace post-rift stratigraphy (e.g. Underhill 1991; Thomson and Underhill 1993; Underhill and Brodie 1993; Davies et al. 2001). The Sronlairig Fault, located onshore south of Loch Ness (Fig. 1a), is a ENE-WSW-trending sinistral fault, considered to have developed initially as a synthetic Riedel to the sinistral Great Glen Fault during the pre-Late Devonian (428 - 390 Ma; Stewart et al. 1999). Kemp et al. (2019) used K–Ar analyses to constrain the timing of the Sronlairig fault. The results suggest two different times of later fault movement at 296 ± 7 (Late Carboniferous–Early Permian) and 145 ± 7 Ma (Late Jurassic–Early Cretaceous), respectively. The former event coincides with a widely recognised dextral shearing event along the Great Glen-Wall Boundary fault in N Scotland, Orkney and Shetland (e.g. see Stewart et al. 1999; Armitage et al. 2020 and references therein). Kemp et al. (2019) suggested that the later age corresponds to the main phase of rifting in the IMFB in the Late Jurassic–Early Cretaceous. They proposed that the Great Glen Fault zone and related structures acted as a northern barrier to active extension at this time, thus explaining the relative absence of deformation at this time in Caithness and the Pentland Firth. Their study further confirms that well known Caledonian faults onshore may have significant Mesozoic movements and may act as barriers or transfer faults connecting or bounding younger offshore basins, as originally suggested by Roberts and Holdsworth (1999).

Our findings support the existence of oblique-dextral N-S- to NNE-SSW-trending faults, some of which are proven to have reactivated Devonian structures in the IMFB, during Hauterivian (130.99 ± 4.60 Ma) rifting. This is somewhat later than

the Berriasian age previously proposed for the cessation of rifting in offshore areas (e.g. Underhill 1990; Davies 2001), but is consistent with studies by Andrews et al. (1990), Roberts et al. (1990) and Argent et al. (2002) all of whom suggest that some faults were longer-lived. The NNW-SSE extension direction deduced from the palaeostress analysis in the present study is parallel to that suggested by Davies et al. (2001) based on offshore fault trends, but the timing proposed by them is Late Jurassic (Oxfordian-early Kimmeridgian) rather than Early Cretaceous. During the late Kimmeridgian-Tithonian, they inferred a change to NE-SW extension in order to explain the development of NW-SW-trending faults in the basin. We suggest that this sequential model should be reassessed and that a synchronous fault development model involving the oblique reactivation of older Orcadian Basin-related structures and the development of new dip-slip faults is also feasible. This would allow multiple fault families to coexist including the main basin to sub-basin-bounding NE-SW dip-slip normal faults, in addition to smaller scale transtensional dextral N-S to NNE-SSW faults, sinistral NW-SE faults and local folds. Oblique kinematics and reactivation of pre-existing structures have certainly been identified elsewhere in the North Sea (e.g. Færseth et al. 1997). More generally, this model is consistent with the suggestion that simple orthogonal rifting models are less common than is generally assumed (e.g. Dewey et al. 1998; Holdsworth et al. 1997; Dichiarante et al. 2020). Further integration of high-resolution offshore 3D seismic reflection data should be used to confirm whether the trends observed onshore in the Turniff Sub-basin can be recognised offshore in the IMFB.

Implications for prospectivity of Devonian-involved plays

In the IMFB, the main reservoir-seal packages are thought to comprise Lower Jurassic to Middle Jurassic sandstones and siltstones interbedded with mudstones.

The Beatrice field (Linsley 1980; Fig. 1b) which was the most significant field in the region, is considered to have been charged by a combination of Devonian and Jurassic source rocks (e.g. Peters et al. 1989; Greenhalgh, 2016). The Devonian source rock in the offshore IMFB is largely thought to lie in the oil window and co-sourcing other fields in the Orcadian Basin (e.g. Greenhalgh 2016). Fractured Devonian sandstones provide known local petroleum reservoirs elsewhere in the North Sea (e.g. Claymore, Buchan, Stirling fields; Marshall and Hewett 2003). Also, the Clair field, West of Shetland is a giant oilfield hosted in fractured Carboniferous-Devonian and Precambrian basement rocks, with a Kimmeridge Clay source (Coney et al. 1993; Holdsworth et al. 2019). The development of reservoir-quality fractured sandstones and local Devonian source rocks in the oil window provide evidence that this type of play could be more extensive. Oil-stained Devonian and basement rocks have certainly been identified in many locations onshore Moray Firth (Greenhalgh 2016 and references therein) and are also locally observed in the highly fractured sandstones at Pennan (Fig. 5d and e).

Our findings show that the Devonian rocks underwent both Devonian and Early Cretaceous deformation, with oblique reactivation of Devonian structures during the later stage. This led to a high density of faults and fracture networks (e.g. Fig. 8c and d.) which are critical for the development of potential Devonian-involved plays. Although there are some similarities in terms of structural style, the reactivation events recognised in the southern part of the former Orcadian Basin are significantly younger than those recognised further to the north (e.g. Caithness, West Orkney Basin).

Conclusions

Our integrated onshore study combines structural studies with absolute U-Pb calcite dating techniques to reveal two main deformation events in the southern part of the superimposed Inner Moray Firth and Orcadian basins.

The earliest event is demonstrably Devonian based on the preservation of growth faulting (Fig. 16a) and is characterised by the development of dip-slip to oblique-sinistral, non-mineralised faults predominantly striking N-S to NNE-SSW. Palaeostress inversion analyses suggest that they developed during ENE-WSW extension and are related to the opening of the Orcadian Basin during sinistral transtensional displacements along the Great Glen Fault. This suggests that the regional tectonic model recognised in the northern part of the Orcadian Basin (e.g. Wilson et al. 2010; Dichiarante et al. 2020) can be extended southwards into the Central Highlands. It is also kinematically compatible with transtensional rifting and strike slip tectonics on the Midland Valley at this time (e.g. Dewey and Strachan 2003).

These early-formed Devonian structures show evidence of later dextral reactivation during a widespread phase of NNW-SSE extension. Also, NE-SW- to WNW-ESE-, and NW-SE- (showing oblique-sinistral kinematics) striking faults and NNW-plunging folds formed at the same time (Fig. 16b). This later deformation is consistently associated with syn-tectonic calcite mineralisation (e.g. shear veins, slickenfibers, tensile veins and Riedel shears). U-Pb calcite dating suggests that the timing of faulting and fault reactivation of pre-existing Devonian structures associated with calcite mineralisation is Early Cretaceous (130.99 ± 4.60 Ma). We consider this to have formed during the latter stages of the more regionally recognised Late Jurassic to Early Cretaceous opening of the IMFB (Davies et al. 2001; Argent et al. 2002). This provides the first clear evidence that strike-slip and oblique-slip faults

coexist in the IMFB during the basin opening. It also provides clear evidence that the main rift-related deformation extends beyond the Banff Fault in the southern part of the IMFB, and into the onshore Turriff Sub-basin, even though younger stratigraphy is not preserved here.

To explain the different fault orientations associated with the Late Jurassic-Early Cretaceous deformation, we favour synchronous development of these structures during transtension and fault reactivation, rather than in-sequence faulting due to stress rotation at different times (as suggested by Davies et al. 2001, for example). Complex fault patterns have been widely associated with transtension and oblique rifting (e.g. Wilson et al. 2006; 2010) and we believe this is the case, at least locally, in the IMFB. Thus, oblique reactivation of pre-existing faults during later rifting episodes leads to the development of highly localised regions of complex deformation that contrast strongly with intervening regions of relatively undeformed, shallowly dipping strata. The scale and kinematics of these structures are directly controlled by the location, scale and orientation of the older inherited faults at depth.

The integration of fieldwork, stress inversion analyses and absolute dating techniques shows that widespread oblique reactivation of earlier Orcadian Basin structures has occurred. This will create reservoir-scale structural heterogeneity in potential Devonian reservoirs and can be used to further explore subsurface Devonian-involved plays elsewhere in the North Sea.

Acknowledgements

This research is based on the PhD work of AT undertaken as part of the Natural Environment Research Council (NERC) Centre for Doctoral Training (CDT) in Oil and Gas [grant number NEM00578X/1] and was funded by Durham University and British Geological Survey (BGS) via the British University Funding Initiative (BUFI), whose support is gratefully acknowledged. We acknowledge the provision of very

thorough review comments by Catherine Mottram, Nick Roberts and Graham Leslie. Ian Chaplin is thanked for his outstanding thin-section preparation. The authors are also grateful to Jack Lee and Nick Roberts (BGS geochronology lab) for attempting calcite dating of some of our samples which unfortunately gave no viable age data. DMC contributes here by permission of the Executive Director, British Geological Survey, UKRI.

References

Allmendinger, R. W., Cardozo, N., and Fisher, D., 2012, Structural geology algorithms: Vectors and tensors in structural geology: Cambridge University Press

Andrews, I.J., Long, D., Richards, P.C., Thomson, A.R., Brown, S., Chesher, J.A. and McCormac, M. 1990 The Geology of the Moray Firth. British Geological Survey, London.

Angelier, J. 1984: Tectonic analysis of fault slip data sets. – Journal of Geophysical Research 89, 5835–5848.

Angelier, J. 1990. Inversion of field data in fault tectonics to obtain the regional stress III: A new rapid direct inversion method by analytical means. – Geophysical Journal International 103, 363–376.

Argent, J., Stewart, S.A., Green, P. and Underhill, J.R. 2002. Heterogeneous exhumation in the Inner Moray Firth, UK North Sea: constraints from new apatite fission track analysis and seismic data. Journal of the Geological Society, 159, 715-729.

Armitage, T. B., Watts, L. M., Holdsworth, R. E. and Strachan, R.A. 2020. Late Carboniferous dextral transpressional reactivation of the crustal-scale Walls Boundary Fault, Shetland: the role of pre-existing structures and lithological heterogeneities, Journal of the Geological Society, 178, https://doi.org/10.1144/jgs2020-078

Ashcroft, W A, and Wilson, C D V. 1976. A geophysical survey of the Turriff basin of Old Red Sandstone, Aberdeenshire. Journal of the Geological Society of London, Vol. 132, 27–43.

Bell, R. E., Jackson, C. A.-L., Whipp, P. S., and Clements, B. 2014. Strain migration during multiphase extension: Observations from the northern North Sea, Tectonics, 33, 1936– 1963, doi:10.1002/2014TC003551

Bird, T. J., Bell, A., Gibbs, A.D., and Nicholson, J., 1987. Aspects of strike-slip tectonics in the Inner Moray Firth Basin, offshore Scotland. Norsk Geologisk Tidsskrift, 67, 353–369.

Bott, M. 1959. The mechanics of oblique slip faulting. Geological Magazine, 96(02):109–117.

Brewer, J. A. and Smythe, D. K. 1984. MOIST and the continuity of crustal reflector geometry along the Caledonian-Appalachian orogen. Journal of the Geological Society, 141(1):105–120.

BGS Moray Firth (Special Sheet). 1995. 1:250 000, Edinburgh, Scotland: British Geological Survey.

BGS. 1987. Fraserburgh, Sheet 97. 1:50 000. Ordnance Survey, Southampton.

Buchan, S. 1932 On some dykes in east Aberdeenshire, Transactions of the Edinburgh Geological Society, 12, 323-328, https://doi.org/10.1144/transed.12.4.323

Cardozo, N., and Allmendinger, R.W., 2013, Spherical projections with OSXStereonet: Computers & Geosciences, v. 51, p. 193 – 205, doi:10.1016/j.cageo.2012.07.021

Coney, D., Fyfe, T.B., Retail, P., and Smith, P.J., 1993, Clair Appraisal - the benefits of a co-operative approach, in Parker, J.R., ed., Petroleum Geology of Northwest Europe: Proceedings of the 4th Conference: Geological Society, London, Petroleum Geology Conference series, v. 4, p. 1409-1420.

Coward, M. P. and Enfield, M. A. 1987. Petroleum geology of north west Europe: London, Heyden & Son, Third Conference on Petroleum Geology of North West Europe Proceedings. In Petroleum geology of north west Europe: London, Heyden & Son, Third Conference on Petroleum Geology of North West Europe Proceedings, pp. 687–696.

Coward, M. P., Enfield, M. A. and Fischer, M. W. 1989. Devonian basins of Northern Scotland: extension and inversion related to Late Caledonian - Variscan tectonics. Geological Society, London, Special Publications, 44(1):275–308.

Davies, R.J., Turner, J.D., and Underhill, J.R., 2001. Sequential dip-slip fault movement during rifting: a new model for the evolution of the Jurassic trilete North Sea rift system. Petroleum Geoscience, 7(4), 371–388, https://doi.org/10.1144/petgeo.7.4.371

De Paola, N., Holdsworth, R.E., McCaffrey, K.J.W. and Barchi, M.R. 2005. Partitioned transtension: an alternative to basin inversion models. Journal of Structural Geology, Volume 27, Issue 4, 2005, 607-625, https://doi.org/10.1016/j.jsg.2005.01.006.

Delvaux, D., Moeys, R., Stapel, G., Petit, C., Levi, K., Miroshnichenko, A., Ruzhich, V., and San'kov, V.: Paleostress reconstructions and geodynamics of the Baikal region, Central Asia, Part 2. Cenozoic rifting, Tectonophysics, Volume 282, Issues 1–4,1997, Pages 1-38, ISSN 0040-1951, https://doi.org/10.1016/S0040-1951(97)00210-2

Dewey, J. F. and Strachan, R. A. 2003. Changing Silurian-Devonian relative plate motion in the Caledonides: sinistral transpression to sinistral transtension. Journal of the Geological Society, 160(2):219–229, https://doi.org/10.1144/0016-764902-085

Dewey, J. F., Holdsworth, R. E. and Strachan, R. A. 1998. Transpression and transtension zones. Geological Society, London, Special Publications, 135(1):1–14.

Dichiarante, A. M., Holdsworth, R. E., Dempsey, E. D., Selby, D., McCaffrey, K. J. W., Michie, U. M., Morgan, G. and Bonniface, J. 2016. New structural and Re-Os geochronological evidence constraining the age of faulting and associated mineralization in the Devonian Orcadian Basin, Scotland. Journal of the Geological Society, pp. 2015–118, https://doi.org/10.1144/jgs2015-118

Dichiarante, A.M., Holdsworth, R.E., Dempsey, E.D., McCaffrey, K.J.W. and Utley, T.A.G. 2020. Outcrop-scale manifestations of reactivation during multiple superimposed rifting and basin inversion events: the Devonian Orcadian Basin, northern Scotland Journal of the Geological Society, 178, jgs2020-089, https://doi.org/10.1144/jgs2020-089

Duncan, W. I. and Buxton, N. W. K. 1995. New evidence for evaporitic Middle Devonian lacustrine sediments with hydrocarbon source potential on the East Shetland Platform, North Sea. Journal of the Geological Society, 152(2):251–258.

Enfield, M. A. and Coward, M. P. 1987. The Structure of the West Orkney Basin, northern Scotland. Journal of the Geological Society, 144(6):871–884, https://doi.org/10.1144/gsjgs.144.6.0871

Færseth, R.B., Knudsen, B.-E., Liljedahl, T., Midbøe, P.S. and Søderstrøm, B. 1997. Oblique rifting and sequential faulting in the Jurassic development of the northern North Sea, Journal of Structural Geology, 19 (10), pp. 1285-1302, https://doi.org/10.1016/S0191-8141(97)00045-X

Fazlikhani, H., Aagotnes, S. S., Refvem, M. A., Wright, J.H., Bell, R. E., Fossen, H., Gawthorpe, R. L., Jackson, C. A-L. and Rotevatn, A. 2020. Strain migration during multiphase extension, Stord Basin, northern North Sea rift, Basin Research, 33: 1474– 1496 https://doi.org/10.1111/bre.12522

Fossen, H., Teyssier, C. and Whitney, D.L. 2013. Transtensional folding, Journal of Structural Geology, Volume 56, Pages 89-102, https://doi.org/10.1016/j.jsg.2013.09.004.

Fournier, M., N. Bellahsen, O. Fabbri, and Gunnell, Y. 2004. Oblique rifting and segmentation of the NE Gulf of Adenpassive margin, Geochem. Geophys. Geosyst., 5, Q11005, doi:10.1029/2004GC000731

Friend, P. F., Williams, B. J., Ford, M. and Williams, E. A. 2000. Kinematics and Dynamics of Old Red Sandstone basins. Geological Society, London, Special Publications, 180(1):29–60.

Frostick, L., Reid, I., Jarvis, J., and Eardley, H. 1988. Triassic sediments of the Inner Moray Firth, Scotland: early rift deposits. Journal of the Geological Society, 145(2), 235–248.

Greenhalgh, E. 2016. Literature Review of Devonian Source Rocks and Devonian-Sourced Hydrocarbons in the Orcadian Basin. British Geological Survey Commissioned Report, CR/16/017. 25pp.

Guariguata-Rojas, G.J and Underhill, J.R. 2017. Implications of Early Cenozoic uplift and fault reactivation for carbon storage in the Moray Firth Basin. Interpretation 5 (4), SS1-SS21

Gunn, A G, Mendum, J R and Thomas, C W. 2015. Geology of the Huntly and Turriff Districts. Sheet description for the 1:50 000 geological sheets 86W (Huntly) and 86E (Turriff) (Scotland), British Geological Survey.

Hansen, J.-A., Bergh, S. G., and Henningsen, T. 2012. Mesozoic rifting and basin evolution on the Lofoten and Vesterålen Margin, North-Norway; time constraints and regional implications. Norwegian Journal of Geology, 91, 203–228, DOI: 10.1111/bre.12358

Healy, D., Rizzo, R. E., Cornwell, D. G., Farrell, N. J. C., Watkins, H., Timms, N. E., et al. 2017. Fracpaq: A MATLAB toolbox for the quantification of fracture patterns. Journal of Structural Geology, 95, 1–16. https://doi.org/10.1016/j.jsg.2016.12.003

Henstra, G.A., Berg Kristensen, T., Rotevatn, A. and Gawthorpe, R.L. 2019. How do pre-existing normal faults influence rift geometry? A comparison of adjacent basins with contrasting underlying structure on the Lofoten Margin, Norway, Basin Res.,31:1083–1097, https://doi.org/10.1111/bre.12358

Hoareau, G., Claverie, F., Pécheyran, C., Paroissin, C., Grignard, P.A., Motte, G., Chailan, O. and Girard, J.P., 2020. Direct U-Pb dating of carbonates from micron scale fsLA-ICPMS images using robust regression. Geochronology Discussion.

Hodgetts, D., Gawthorpe, R.L., Wilson, P., and Rarity, F. 2007. Integrating digital and traditional field techniques using virtual reality geological studio (VRGS), Society of Petroleum Engineers e 69th European Association of Geoscientists and Engineers Conference and Exhibition 2007. Securing the Future, 83-87.

Holdsworth, R. E., Butler, C. A. and Roberts, A. M. 1997. The recognition of reactivation during continental deformation. Journal of the Geological Society, 154(1):73–78.

Holdsworth, R.E., McCaffrey, K.J.W., Dempsey, E., Roberts, N.M.W., Hardman, K., Morton, A., Feely, M., Hunt, J., Conway, A., Robertson, A. 2019. Natural fracture propping and earthquake-induced oil migration in fractured basement reservoirs. *Geology*, v 47, 700-704. https://doi.org/10.1130/G46280.1

Hurst, A R. 1981. Mid Jurassic Stratigraphy and Facies at Brora, Sutherland, Scottish Journal of Geology, 17, 169-177, https://doi.org/10.1144/sjg17030169

Johnstone, G. S. and Mykura, W. 1989. British regional geology: the Northern Highlands of Scotland, vol. 2. HM Stationery Office.

Kamb, W. B. 1959. Ice petrofabric observations from Blue Glacier, Washington, in relation to theory and experiment, J. Geophys. Res., 64(11), 1891– 1909, doi:10.1029/JZ064i011p01891.

Kemp, S., Gillespie, M., Leslie, G., Zwingmann, H., and Campbell, S. 2019. Clay mineral dating of displacement on the Sronlairig Fault: Implications for Mesozoic and Cenozoic tectonic evolution in northern Scotland. Clay Minerals, 54(2), 181-196, doi:10.1180/clm.2019.25

Kylander-Clark, A.R., 2020. Expanding the limits of laser-ablation U–Pb calcite geochronology. Geochronology, 2(2), pp.343-354.

Lăpădat, A., Imber, J., Yielding, G., Iacopini, D., McCaffrey, K. J. W., Long, J. J. and Jones, R. R. 2016. Occurrence and development of folding related to normal faulting within a mechanically heterogeneous sedimentary sequence: a case study from Inner Moray Firth, UK, Geological Society, London, Special Publications, 439, 373-394, https://doi.org/10.1144/SP439.18

Le Breton, E., Cobbold, P.R., and Zanella, A., 2013. Cenozoic reactivation of the Great Glen Fault, Scotland: additional evidence and possible causes. Journal of the Geological Society, 170(3), 403–415.

Linsley, P.N., Potter, H.C., Mcnab, G. and Racher, D. 1980. The Beatrice field, Inner Moray Firth, U.K. North Sea. In: Halbouty, M. T. (ed.) Giant oil and gas fields of the decade 1968-1978. Memoir of the American Association of Petroleum Geologists, 30, 117-29.

Long, J.J. and Imber, J. 2010. Geometrically coherent continuous deformation in the volume surrounding a seismically imaged normal fault-array. Journal of Structural Geology, 32, 222–234. https://doi.org/10.1016/j.jsg.2009.11.009

Lovecchio, J.P., Rohais, S., Joseph, P, Bolatti, N. D., Kress, P. R., Gerster, R. and Ramos, V. A. 2018. Multistage rifting evolution of the Colorado basin (offshore Argentina): Evidence for extensional settings prior to the South Atlantic opening. Terra Nova. 30: 359– 368. https://doi.org/10.1111/ter.12351

Macgregor, D. 2015 History of the development of the East African Rift System: A series of interpreted maps through time, Journal of African Earth Sciences, Volume 101, Pages 232-252, https://doi.org/10.1016/j.jafrearsci.2014.09.016

Marshall, J.E.A. and Hewett, A.J. 2003. Devonian. In: Evans, D., Graham, C., Armour, A. and Bathurst, P., Millennium Atlas: Petroleum Geology of the Northern North Sea. Geological Society, London, 64–81.

McArthur, A.D., Hartley, A.J. and Jolley, D.W. 2013. Stratigraphic development of an Upper Jurassic deep marine syn-rift succession, Inner Moray Firth Basin, Scotland. Basin Res, 25: 285-309. https://doi.org/10.1111/j.1365-2117.2012.00557.x

McCaffrey, K.J.W., Jones, R.R., Holdsworth, R.E., Wilson, R.W., Clegg, P., Imber, J., Holliman, N. and Trinks, I. 2005. Unlocking the spatial dimension: digital technologies and the future of geoscience fieldwork, Journal of the Geological Society, 162, 927-938, 1, https://doi.org/10.1144/0016-764905-017

McClay, K., Norton, M. G., Coney, P., Davis, G. H. et al. 1986. Collapse of the Caledonian orogen and the Old Red Sandstone, Nature 323, 147–149 https://doi.org/10.1038/323147a0

McQuillin, R., Donato, J.A., and Tulstrup, J. 1982. Development of basins in the Inner Moray Firth and the North Sea by crustal extension and dextral displacement of the Great Glen Fault. Earth and Planetary Science Letters, 60(1), 127–139.

Michael, A. J. 1984. Determination of stress from slip data: faults and folds. Journal of Geophysical Research: Solid Earth (1978–2012), 89(B13):11517–11526.

Mostafa, M. E. 2005: Iterative direct inversion: An exact complementary solution for inverting fault-slip data to obtain palaeostresses. Computers & Geosciences, v. 31. https://doi.org/10.1016/j.cageo.2005.02.012

NIREX. 1994a. The Geology of the Region Around Dounreay: Report of the Regional Geology Joint Interpretation Team. UK Nirex Limited Report, 657.

Norton, M. J., Mcclay, K. R. and Nick, A. W. 1987. Tectonic evolution of Devonian basins in northern Scotland and southern Norway. Norsk Geologisk Tidsskrift, 67:323.

Passchier, C. and Trouw, R. 2005. Microtectonics. 366 pp. Springer, Berlin.

Peters, K. E., Moldowan, J. M., Driscole, A. R. and Demaison, G. J. 1989. Origin of Beatrice Oil by Co-Sourcing from Devonian and Middle Jurassic Source Rocks, Inner Moray Firth, United Kingdom. AAPG Bulletin; 73 (4): 454–471. doi: https://doi.org/10.1306/44B49FCE-170A-11D7-8645000102C1865D

Petit, J. P., 1987, Criteria for the sense of movement on fault surfaces in brittle rocks: Journal of Structural Geology, v. 9, p. 597–608.

Pickering K. T. 1984. The Upper Jurassic 'Boulder Beds' and related deposits: a fault-controlled submarine slope, NE Scotland, Journal of the Geological Society, 141, 357-374, https://doi.org/10.1144/gsjgs.141.2.0357

Ragon, T., Nutz, A., Schuster, M., Ghienne, J.F., Ruffet, G. and Rubino, J.L. 2018 Evolution of the northern Turkana Depression (East African Rift System, Kenya) during the Cenozoic rifting: New insights from the Ekitale Basin (28-25.5Ma). Geological Journal, 54, 3468–3488, https://doi.org/10.1002/gj.3339

Ramsay, J. 1980. The crack–seal mechanism of rock deformation. Nature 284, 135–139, https://doi.org/10.1038/284135a0

Read, H H. 1923. The geology of the country around Banff, Huntly and Turriff (Lower Banffshire and North-west Aberdeenshire) Explanation of Sheets 86 and 96. Memoir of the Geological Survey, Scotland. (Edinburgh: HMSO).

Roberts, A.M., and Holdsworth R.E. 1999. Linking onshore and offshore structures: Mesozoic extension in the Scottish Highlands. Journal of the Geological Society, 156, 1061–1064.

Roberts, A.M., Badley, M.E., Price, J. D., and Huck, I.W. 1990. The structural history of a transtensional basin: Inner Moray Firth, NE Scotland. Journal of the Geological Society, 147(1), 87–103.

Roberts, N. M. W., Lee, J. K., Holdsworth, R. E., Jeans, C., Farrant, A. R., and Haslam, R. 2020. Near-surface Palaeocene fluid flow, mineralisation and faulting at Flamborough Head, UK: new field observations and U-Pb calcite dating constraints, Solid Earth, https://doi.org/10.5194/se-11-1931-2020

Roberts, N.M., Drost, K., Horstwood, M.S., Condon, D.J., Chew, D., Drake, H., Milodowski, A.E., McLean, N.M., Smye, A.J., Walker, R.J. and Haslam, R., 2020. Laser ablation inductively coupled plasma mass spectrometry (LA-ICP-MS) U–Pb carbonate geochronology: strategies, progress, and limitations. Geochronology, 2, 33-61.

Rogers, D. A., Marshall, J. E. A. and Astin, T. R. 1989. Short Paper: Devonian and later movements on the Great Glen fault system, Scotland. Journal of the Geological Society, 146(3):369–372.

Rotevatn, A., Kristensen, T. B., Ksienzyk, A. K., Wemmer, K., Henstra, G. A., Midtkandal, I., Grundvåg, S.-A., and Andresen, A. 2018. Structural inheritance and rapid rift-length establishment in a multiphase rift: The East Greenland rift system and its Caledonian orogenic ancestry. Tectonics, 37, 1858–1875. https://doi.org/10.1029/2018TC005018

Sasvári, Á. and Baharev, A. 2014: SG2PS (structural geology to post script converter) – A graphical solution for brittle structural data evaluation and paleostress calculation. – Computers & Geosciences 66, 81–93.

Seranne, M. 1992. Devonian extensional tectonics versus Carboniferous inversion in the northern Orcadian basin. Journal of the Geological Society, 149(1):27–37.

Spang J. 1972. Numerical method for dynamic analysis of calcite twin lamellae. Geol Soc Am Bull 84:134–150.

Steel, R. and Ryseth, A. 1990. The Triassic — early Jurassic succession in the northern North Sea: megasequence stratigraphy and intra-Triassic tectonics, Geological Society, London, Special Publications, 55, 139-168, https://doi.org/10.1144/GSL.SP.1990.055.01.07

Stephenson, D. and Gould, D. 1995. The Grampian Highlands, 4th ed. British Regional Geology Series, x 261 pp. London: HMSO for the British Geological Survey. ISBN 0 11 884521 7. Geological Magazine, 133(4), 506-506. doi:10.1017/S0016756800007779

Stewart, M., Strachan, R. A., and Holdsworth, R. E. 1999. Structure and early kinematic history of the Great Glen Fault Zone, Scotland, Tectonics, 18(2), 326–342, doi:10.1029/1998TC900033

Stoker, M. S., Hitchen, K. and Graham, C. C. 1993. The geology of the Hebrides and West Shetland shelves, and adjacent deep-water areas, vol. 2. The Stationery Office/Tso.

Sweet, I. 1895. The sedimentology of the Lower Old Red Sandstone near New Aberdour, Grampian Region, *Scottish Journal of Geology*, **21,** 239-259, 1985, https://doi.org/10.1144/sjg21030239

Tămaș, D. M., Tămaș, A., Barabasch, J., Rowan, M. G., Schleder, Z., Krézsek, C., and Urai, J. L. 2021. Low-angle shear within the exposed Mânzălești diapir, Romania: Salt decapitation in the Eastern Carpathians fold-and-thrust belt. Tectonics, 40, e2021TC006850. https://doi.org/10.1029/2021TC006850

Thomson, K. and Hillis, R.R. 1995. Tertiary structuration and erosion of the Inner Moray Firth. In: Scrutton, R.A., Stoker, M.S., Shimmield, G.B. and Tudhope, A.W. The Tectonics, Sedimentation and Palaeoceanography of the North Atlantic Region. Geological Society, London, Special Publications, 90, 249–269.

Thomson, K., and Underhill, J.R. 1993. Controls on the development and evolution of structural styles in the Inner Moray Firth Basin. Petroleum Geology of Northwest Europe: Proceedings of the 4th Conference on Petroleum Geology of NW. Europe, London, 1167–1178.

Tomasso, M., Underhill, J.R., Hodgkinson, R.A. and Young, M.J. 2008. Structural styles and depositional architecture in the Triassic of the Ninian and Alwyn North fields: Implications for basin development and prospectivity in the Northern North Sea. Marine and Petroleum Geology, 25, 588-605

Trewin, N. and Hurst, A. 2009. Excursion Guide to the Geology of East Sutherland and Caithness, 2nd ed. Aberdeen Geological Society and Dunedin Press.,Geological Magazine, 147(5), 798-799.

Trewin, N.H. 1987. Pennan, unconformity within the Old Red Sandstone, Excursion 8, *In: Excursion guide to the geology of the Aberdeen area*, edited by: Trewin, N.H.T, Kneller, B.C. and Gillen, C., Scottish Academic Press, Edinburgh, 127-130, 1987.

Trewin, N.H.T., Andrews S. D. and Kneller, B.C. 1987. The Lower Old Red Sandstone of New Aberdour, edited by: Trewin, N.H.T, Kneller, B.C. and Gillen, C., Scottish Academic Press, Edinburgh.

Underhill, J.R. and Partington, M.A. 1993. Jurassic thermal doming and deflation: the sequence stratigraphic evidence. In: Parker, J.R. (Ed.): Petroleum Geology of North-West Europe: Proceedings of the 4th Conference, 337-345.

Underhill, J.R. 1991. Implications of Mesozoic - Recent basin development in the western Inner Moray Firth, UK. Marine and Petroleum Geology, 8, 359–369.

Underhill, J.R. and Brodie, J.A. 1993. Structural geology of Easter Ross, Scotland: implications for movement on the Great Glen fault zone, 150, 515–527.

Vermeesch, P. 2018. IsoplotR: a free and open toolbox for geochronology. Geoscience Frontiers, v.9, p.1479-1493, doi:10.1016/j.gsf.2018.04.001.

Wallace, R. E. 1951. Geometry of shearing stress and relation to faulting. The Journal of Geology, pp. 118–130.

Watts, L. M., Holdsworth, R. E., Sleight, J. A., Strachan, R. A. and Smith, S. A. F. 2007. The movement history and fault rock evolution of a reactivated crustal-scale strike-slip fault: the Walls Boundary Fault Zone, Shetland. Journal of the Geological Society, 164(5):1037–1058.

Weismüller, C., Urai, J. L., Kettermann, M., von Hagke, C., and Reicherter, K. 2019. Structure of massively dilatant faults in Iceland: lessons learned from high-resolution unmanned aerial vehicle data. Solid Earth, 10, 1757–1784. https://doi.org/10.5194/se-10-1757-2019

Whiteman, A., Naylor, D., Pegrum, R. and Rees, G., 1975. North Sea Troughs and plate tectonics. Tectonophysics, 26: 39-54, https://doi.org/10.1016/0040-1951(75)90112-2

Wilson R.W., Holdsworth R.E., Wild L.E., McCaffrey K.J.W., England, R.W, Imber, J. and Strachan, R.A. 2010. Basement influenced rifting and basin development: a reappraisal of post-Caledonian faulting patterns from the North Coast Transfer Zone, Scotland. Geological Society, London, Special Publications 335, 795–826.

Wilson, R. W., Mccaffrey, K. J. W., Holdsworth, R. E., Imber, J., Jones, R. R., Welbon, A. I. F. and Roberts, D. 2006. Complex fault patterns, transtension and structural segmentation of the Lofoten Ridge, Norwegian margin: Using digital mapping to link onshore and offshore geology. Tectonics, 25(4). http://dx.doi.org/10.1029/2005TC001895

Woodcock, N. H. and Strachan, R. A. 2012. Geological history of Britain and Ireland. John Wiley & Sons, Ltd.

Zanella, E. and Coward, M. P. 2003. Structural Framework. In: Evans, D., Graham, C., Armour, A., and Bathurst, P. (eds) The Millennium Atlas: Petroleum Geology of the Central and Northern North Sea. Geological Society of London, 45-59.

Zanella, E., Coward, M. P., and McGrandle, A. 2003. Crustal structure. In: Evans, D., Graham, C., Armour, A., and Bathurst, P. (eds) The Millennium Atlas: Petroleum Geology of the Central and Northern North Sea. Geological Society of London, 35–42.

Figure Captions

Figure 1: (a) Simplified tectonic map of Scotland and the North Sea showing the main fault systems (after Roberts and Holdsworth 1999; Zanella and Coward 2003 and Kemp et al. 2019). The faults mentioned in the text are shown in red. GGFZ, Great Glen Fault Zone. Outline of the Orcadian Basin marked in dotted orange line (after Duncan and Buxton, 1995) (b) Regional geological map of northern Scotland and associated offshore regions showing the main stratigraphy and fault systems (modified after Guariguata-Rojas and Underhill 2017 and British Geological Survey (BGS), UK. Using: EDINA Geology DigimapService, <http://edina.ac.uk/digimap. IMFB, Inner Moray Firth Basin. (c) Geological map of the Turriff sub-basin (modified after British Geological Survey (BGS), UK. Using: EDINA Geology DigimapService, <http://edina.ac.uk/digimap). Yellow stars show location of the areas of study.

Figure 2: Left-hand column shows the general stratigraphy of the IMFB (modified after Trewin and Hurst 2009) with details concerning the Devonian sequence redrawn after Gunn et al. (2015) shown in the inset right-hand column. Not to scale, with relative thicknesses shown being notional.

Figure 3: (a) Aerial (using EdinaDigimap service © Getmapping Plc) and (b) geological map of Pennan. Field data supplemented with data digitised after Trewin

1987. (c, d) Stereonets and rose plots of structural data collected in the field. Lower hemisphere, equal area projections. The locations of Figures 4-6 are also shown in (a).

Figure 4: Cliff exposure below the Nethermill Cottages, location indicated on Fig. 3a. (a) 3D digital outcrop and inset lower hemisphere equal area stereonets derived from planes extracted from 3D photogrammetric model. Main faults are highlighted in white with senses of offset where known. Lineations on fault plane are shown with yellow lines. Locations of (b) and (c) are indicated by the yellow box. (b) Field photograph and (c) line drawing showing a cross-sectional view looking SW onto the angular unconformity between the Lower and Middle Devonian and main faults with growth strata in their hangingwall. Note the low-angle fault at the base of the outcrop. The location of Figure 5a is shown by the yellow box.

Figure 5: Non-mineralised faults and fractures at Pennan locality. (a) Oblique view showing growth packages within the tilted Lower Devonian sequence. The non-mineralised faults are highlighted in red (see location on Fig. 4b). (b) Stereonet and rose plot of the non-mineralised faults and fractures at Pennan. (c) Sketch explaining the presence of growth strata in the footwall of the bright red coloured fault in Figs 4 and 5a (d) Field photographs showing low angle and listric faults in the Lower Devonian exposure at Pennan Harbour (see location on Fig. 3a). (e) Oblique view of an exposed non-mineralised fault plane showing dip-slip kinematics. In places, oil stains are visible on the fault/fracture planes.

Figure 6: Calcite mineralised faults, fractures and associated structures at the Pennan locality. (a) Cross section view of a N-S-trending calcite-mineralised fault. (b) Detailed image of calcite mineralised breccia in the fault core. c) Stereonet and rose

plot of calcite mineralised faults and fractures (lower hemisphere, equal area projection). d) Oblique view and sketch of tensile calcite veins associated with a N-S-trending fault indicating dextral slip along the fault.

Figure 7: (a) Aerial map (using EdinaDigimap service © Getmapping Plc) and (b) geological map of New Aberdour. Lithology data digitised after Sweet, 1985: from younger to older: 1 - sandstones and siltstones; 2 - sandy mudstone, mudstone, limestone; 3 - coarse to fine sandstone; 4 - conglomeratic sandstone; 5 - conglomeratic sandstone with trough cross bedding; 6 – breccia. (c) Stereonets of structural data collected in the field. Lower hemisphere, equal area projections. Locations of Figures 8, 9a, b and 12 are also shown in (a).

Figure 8: Overview and lineament interpretation of the western side of New Aberdour Bay. Location of the area shown in Fig 10a is also shown. (a) Orthomosaic model obtained from UAV (Unmanned Aerial Vehicle) photography. (b) DEM model, providing high resolution image for lineament interpretation. Orthomosaic models and inset rose diagram showing lineaments of (c) more than ~10m length and (d) less than ~10m length.

Figure 9: Example of non-mineralised structures recognised at New Aberdour locality (see location on Fig. 7a). (a) Section view of normal fault showing about 50 cm of displacement with minor quantities of green fault gouge. (b) Oblique view of clean break fault plane showing dip-slip lineations and grooves. (c) Equal area lower hemisphere stereonet and rose plot of non-mineralised faults and fractures at New Aberdour locality.

Figure 10: Examples of faulting and associated structures cross-cutting the Devonian sandstones and Dalradian basement in the western part of the New

Aberdour Bay. For location see Fig 8a. a) Orthomosaic obtained from UAV (Unmanned Aerial Vehicle) photography, illustrating dextral reactivated NNE-SSW striking faults (red), oblique sinistral NW-SE striking faults (white) Bedding and fold axial traces are highlighted in orange b) NW-plunging tight folds c) Clean break N-S fault plane showing early dip-slip slickenlines and d) overprinting oblique-dextral calcite slickenfibers with the location of the S01 sample shown.

Figure 11: Examples of calcite mineralised structures from the New Aberdour locality. a) Plan view of a minor calcite-mineralised dextral fault associated with the major NNE-SSW-trending fault (Fault I in Fig 10a). b) Close-up of the calcite slickenfibers on the fault plane showing dextral slip with the location of the S02 sample shown. c) Oblique view of other calcite mineralised N-S-to NNE-SSW-trending dextral faults (white) offsetting bedding (orange). d) Stereonet (lower hemisphere, equal area projection) and rose plot of calcite mineralised structures.

Figure 12: a) Aerial image and line drawing showing folded strata on the eastern side of the bay. b) Stereonet showing poles to bedding and the hinge lines of the folds. c) Oblique field photograph showing the folded layers looking northeastwards.

Figure 13: Photomicrographs of textures associated with calcite mineralised faults discussed in the text – all images here cut parallel to local slickenline/fibre lineations in the samples and are in plane polarized light. Red arrows show senses of shear, whilst yellow arrows show local opening and fibre directions. (a, b) Stacked shear and dilational veins in samples S03 and S01, respectively. Note oblique fibres in (b) consistent with dextral shear. (c) High power view of fibres with aligned crack-seal inclusion trails and healed microfractures – note obliquity consistent with dextral shear. Sample S01. (d, e) ‘Feathered dilational vein arrays associated with gouge-

bearing shear fractures consistent with dextral shear in the dated sample S02. (f) Sheared Devonian siltstone and carbonate in dated sample S02 with dextral Riedel/shear bands.

Figure 14: a) Isotopic concentration maps of ^{238}U, ^{206}Pb and ^{24}Mg generated using LA-ICP-MS trace element mapping in sample S02. b) Tera–Wasserburg diagram of measured in-situ calcite $^{207}Pb/^{206}Pb$ and $^{238}U/^{206}Pb$ ratios (no common lead correction) from sample S02 (second cycle of the Manndrapselva Member) yielding a Model I discordia age of 130.99 ± 4.60 Ma (2σ, MSWD = 0.17; See text for discussion).

Figure 15: Stress inversion plots (after Angelier 1990) for: a) non-mineralised; and b) calcite mineralised structures.

Figure 16: Summary of the structural history and schematic block diagrams illustrating the superimposed basin development during (a) Devonian and (b) Late Jurassic-Early Cretaceous.

Figure 1

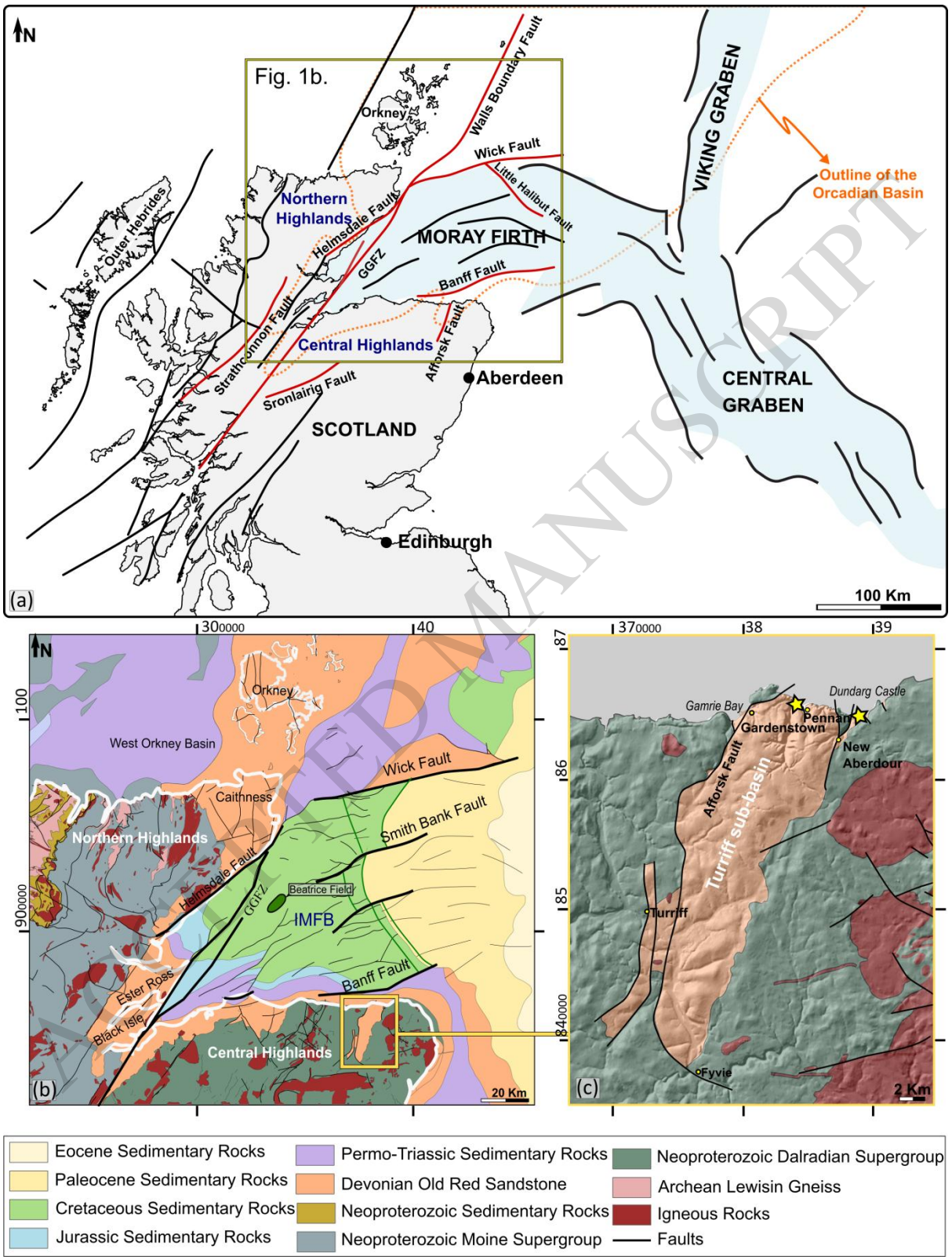

Figure 2

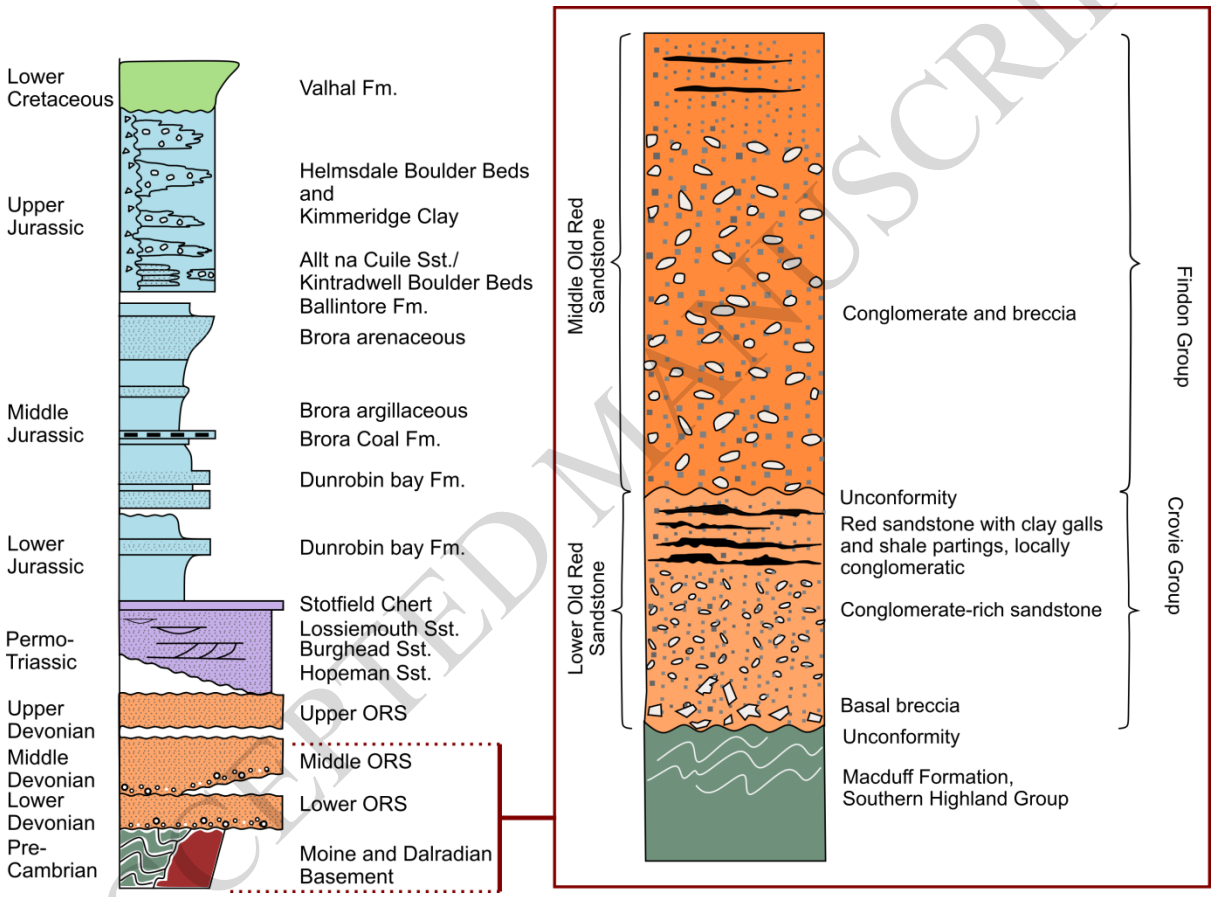

Figure 3

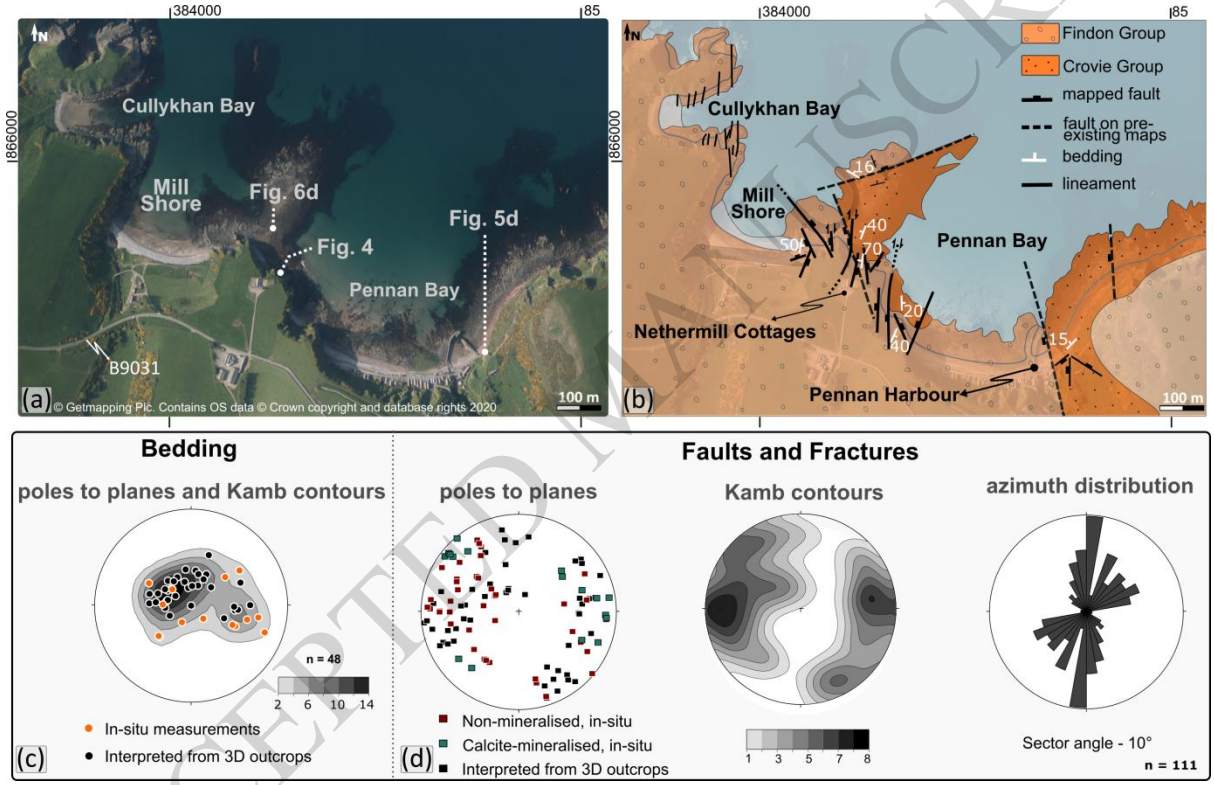

Figure 4

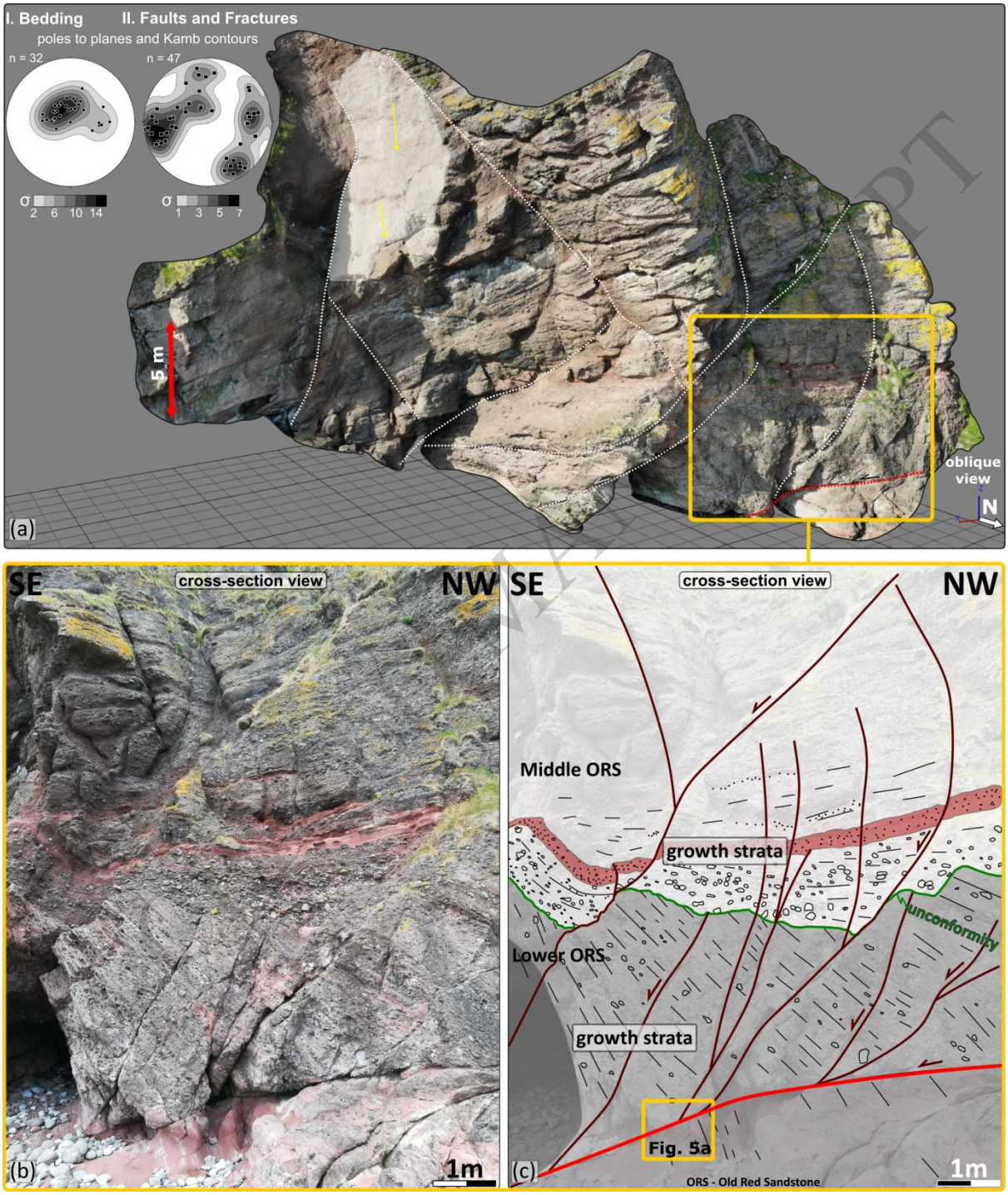

Figure 5

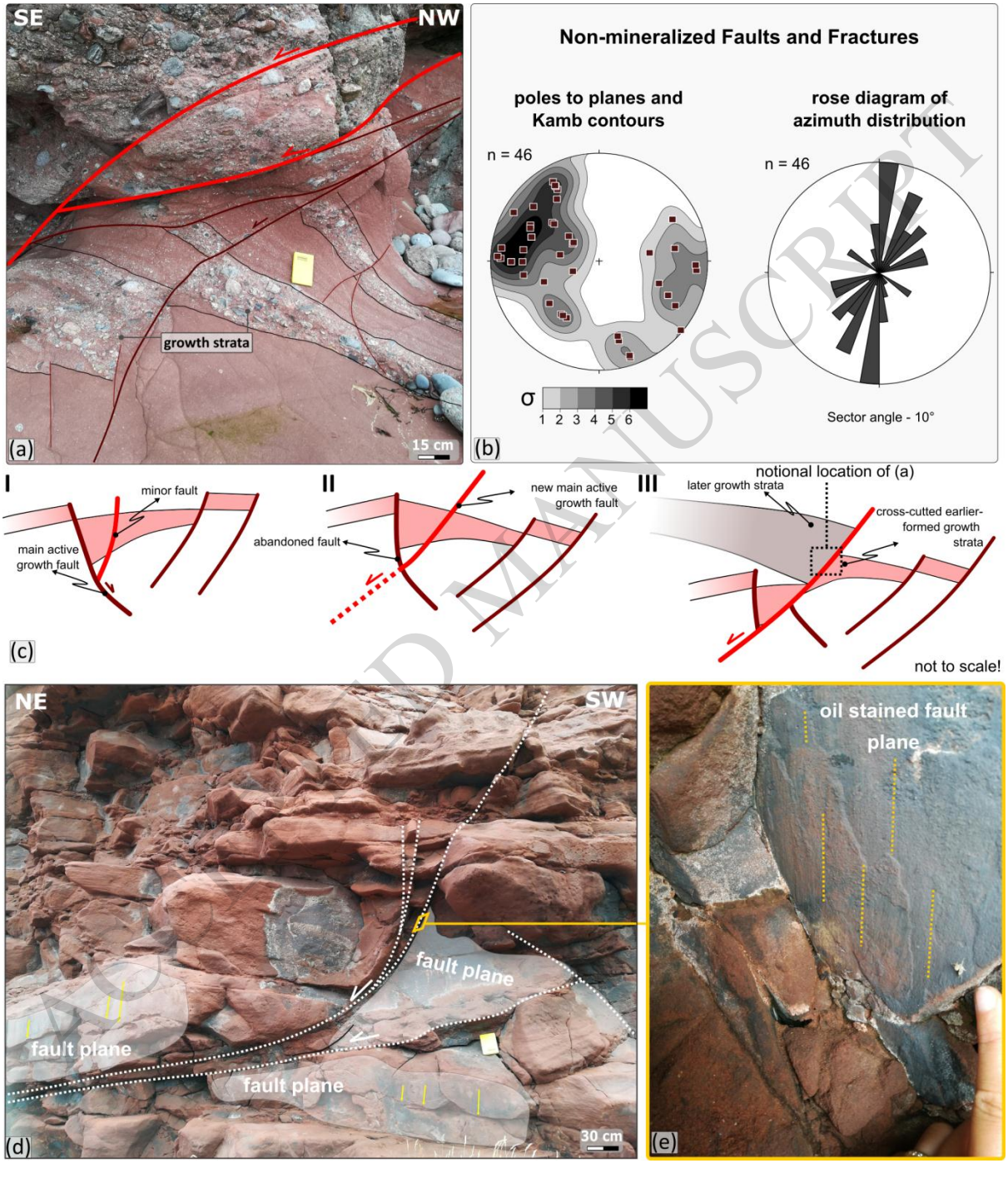

Figure 6

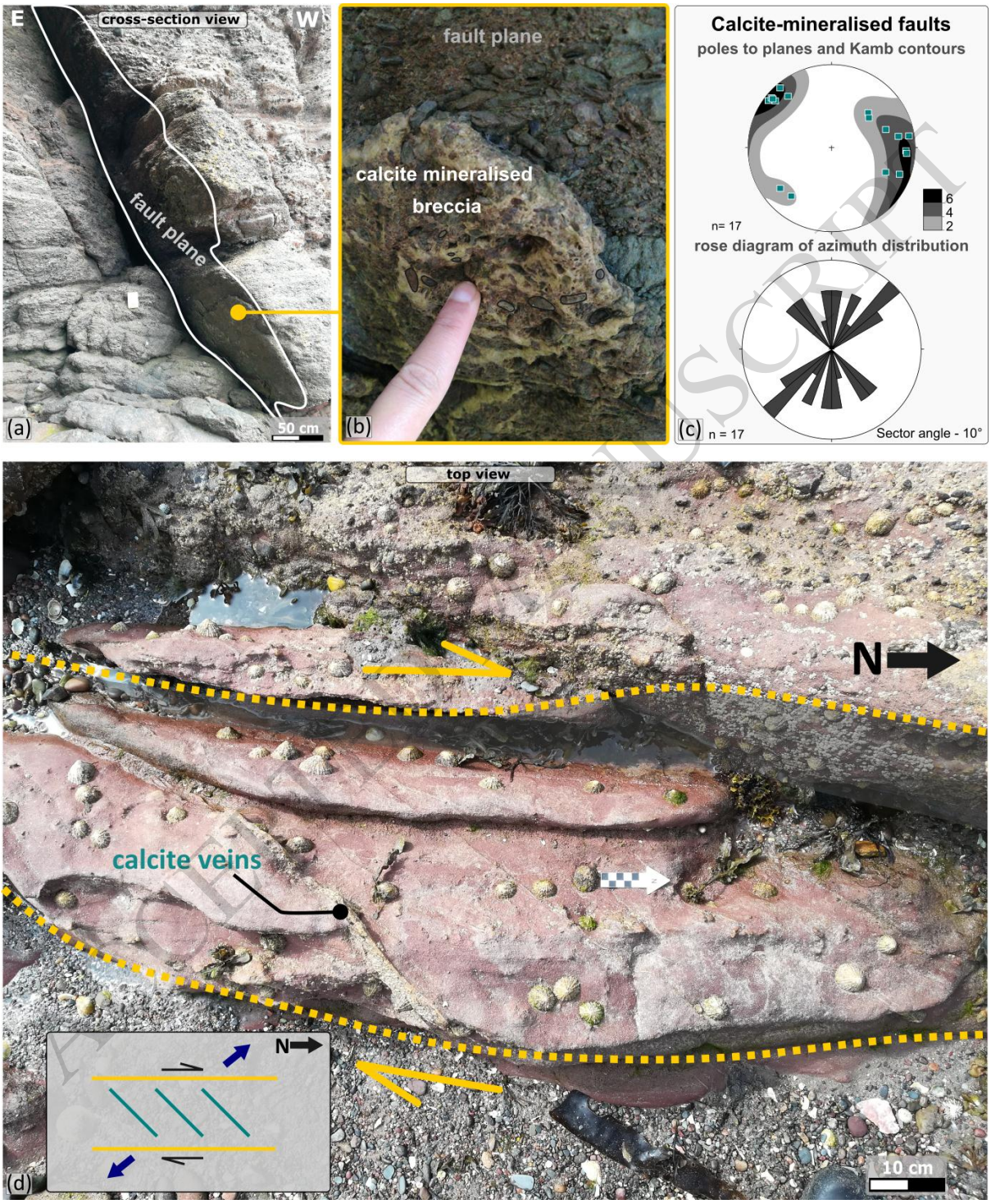

Figure 7

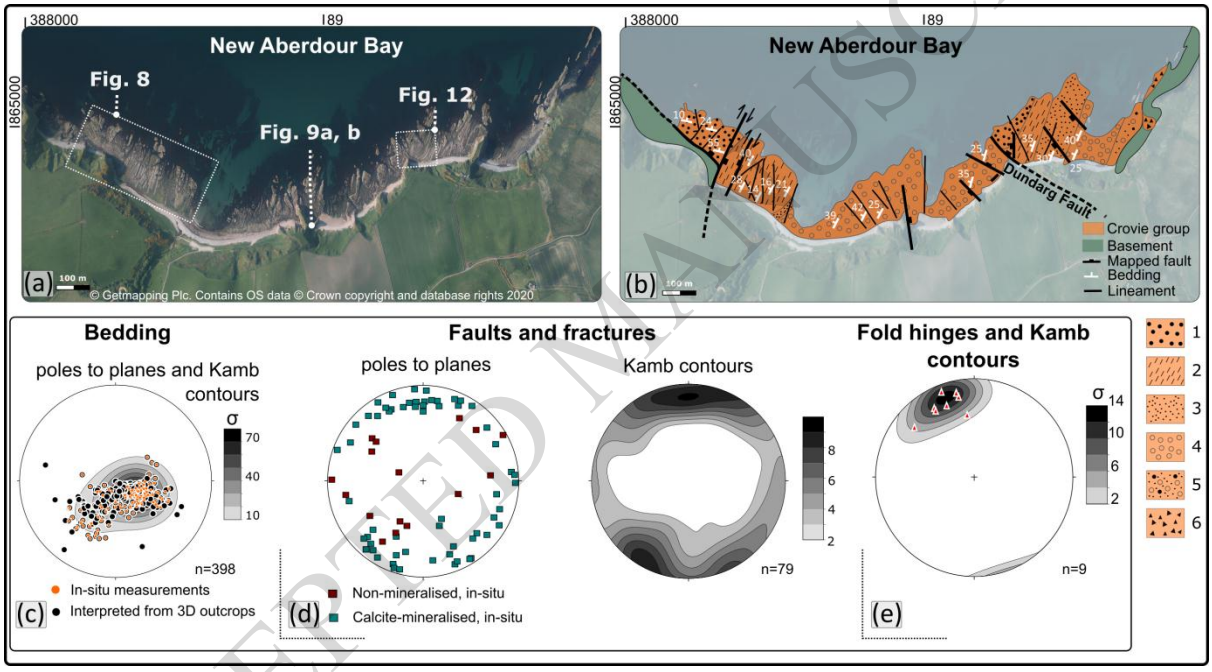

Figure 8

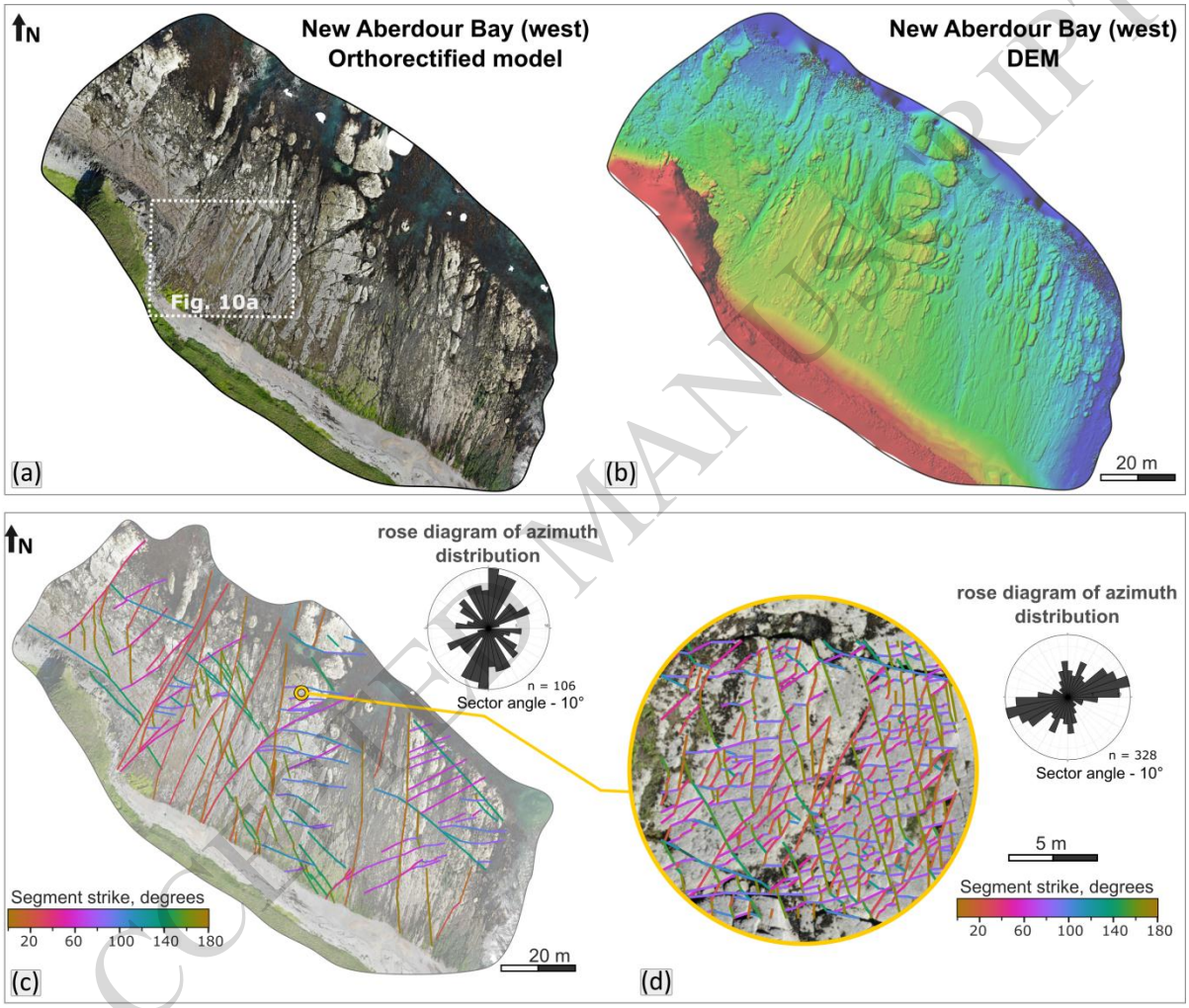

Figure 9

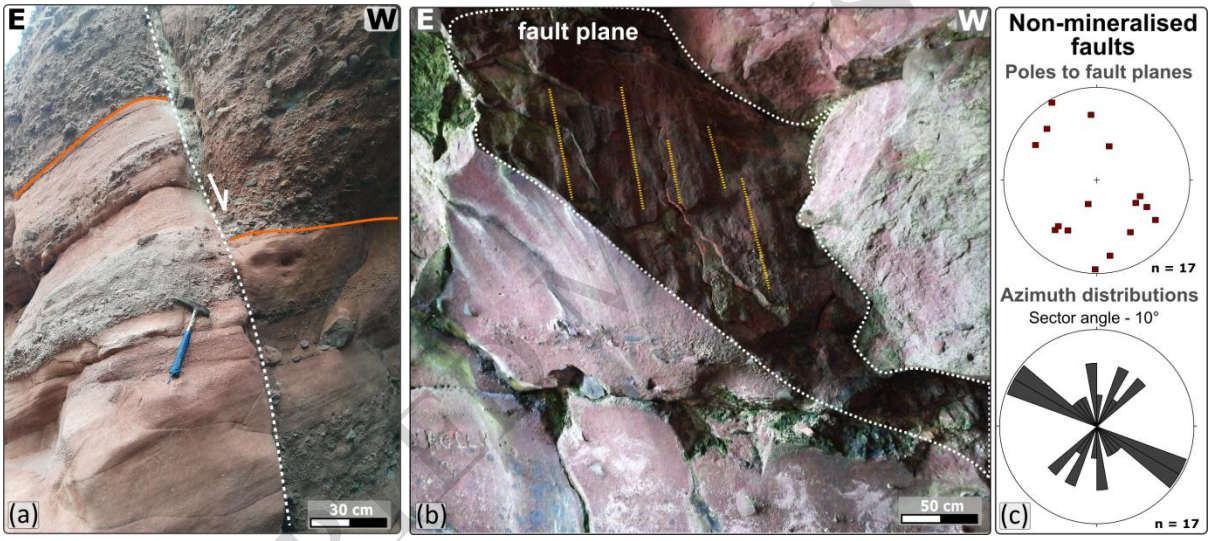

Figure 10

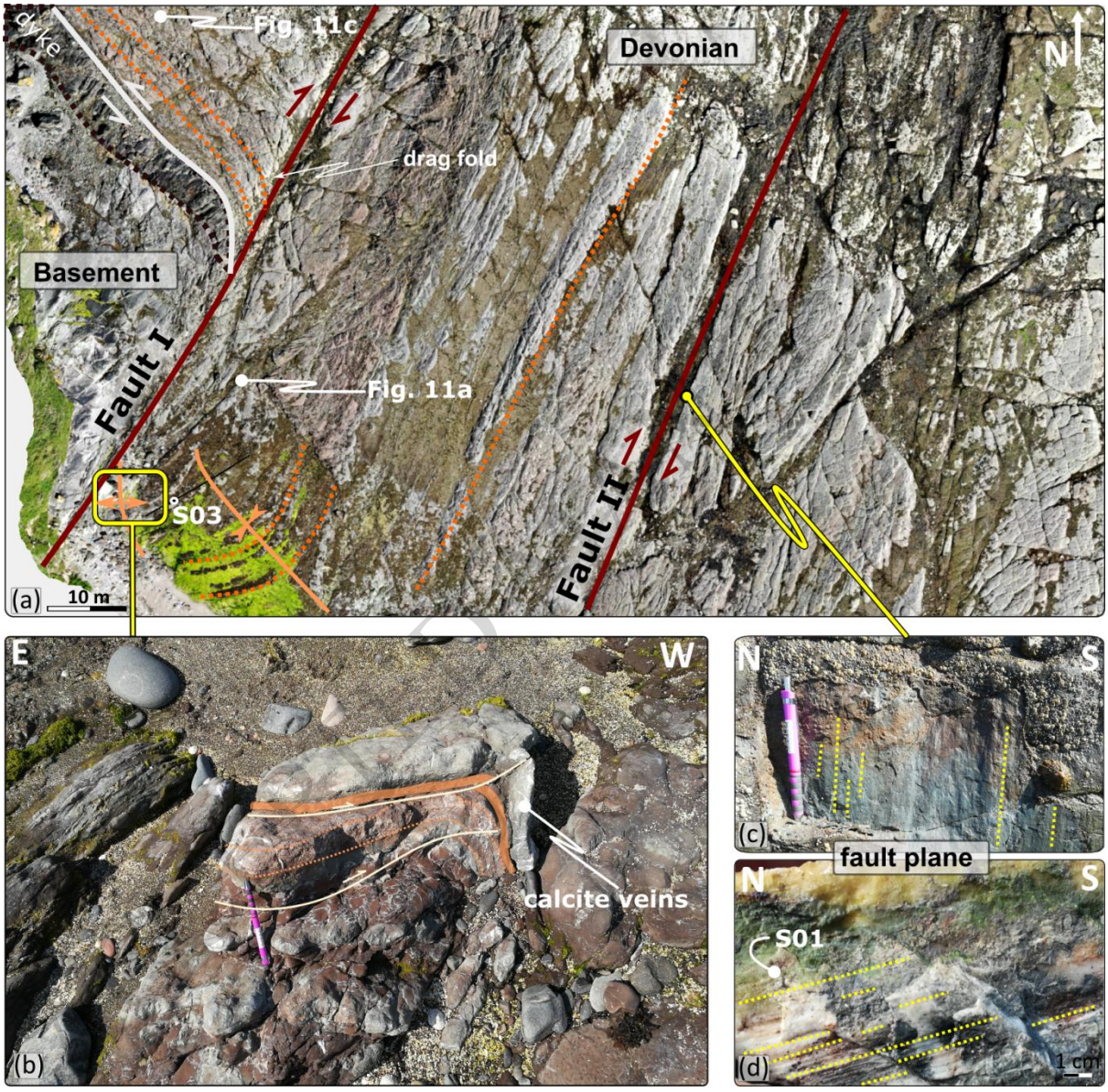

Figure 11

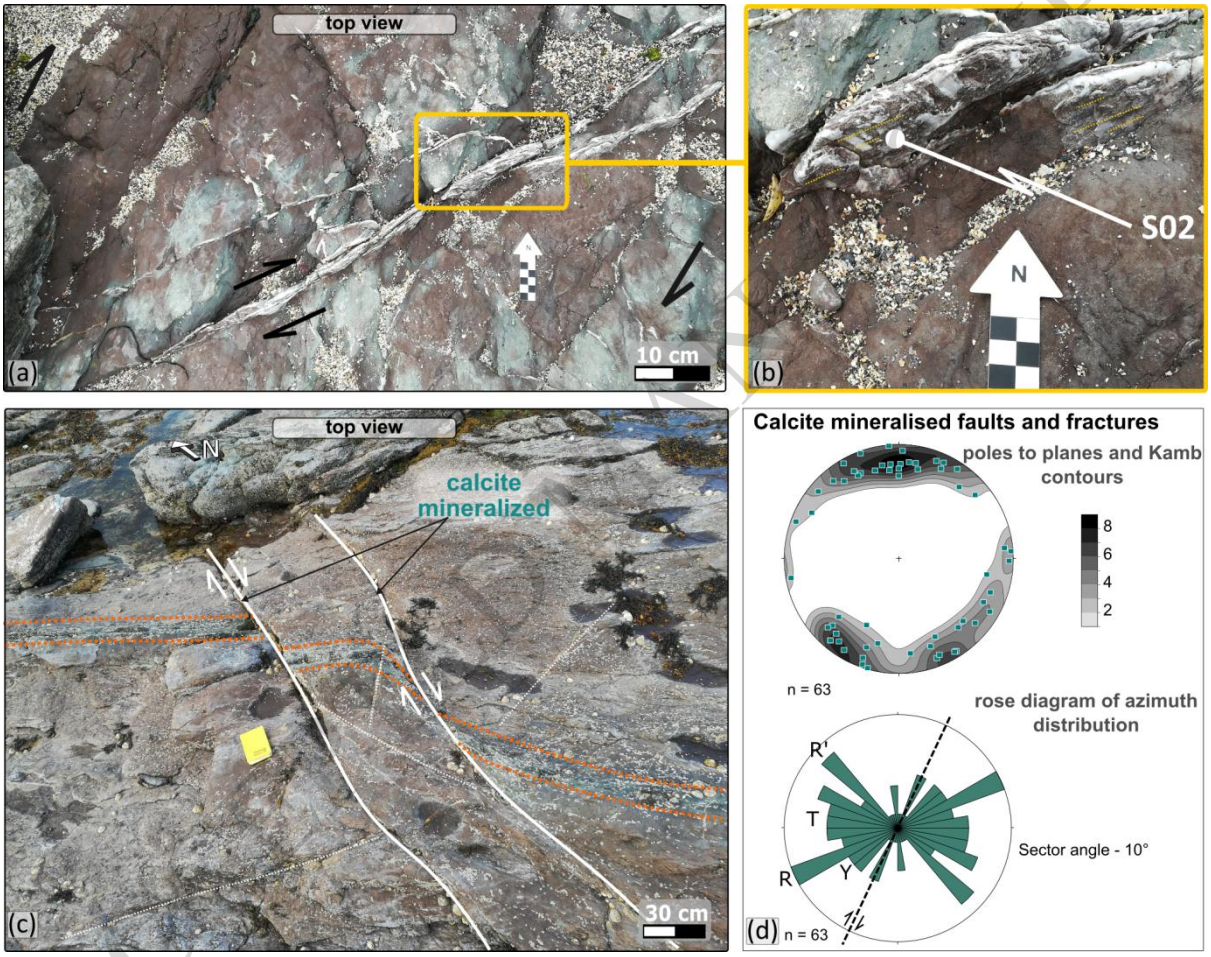

Figure 12

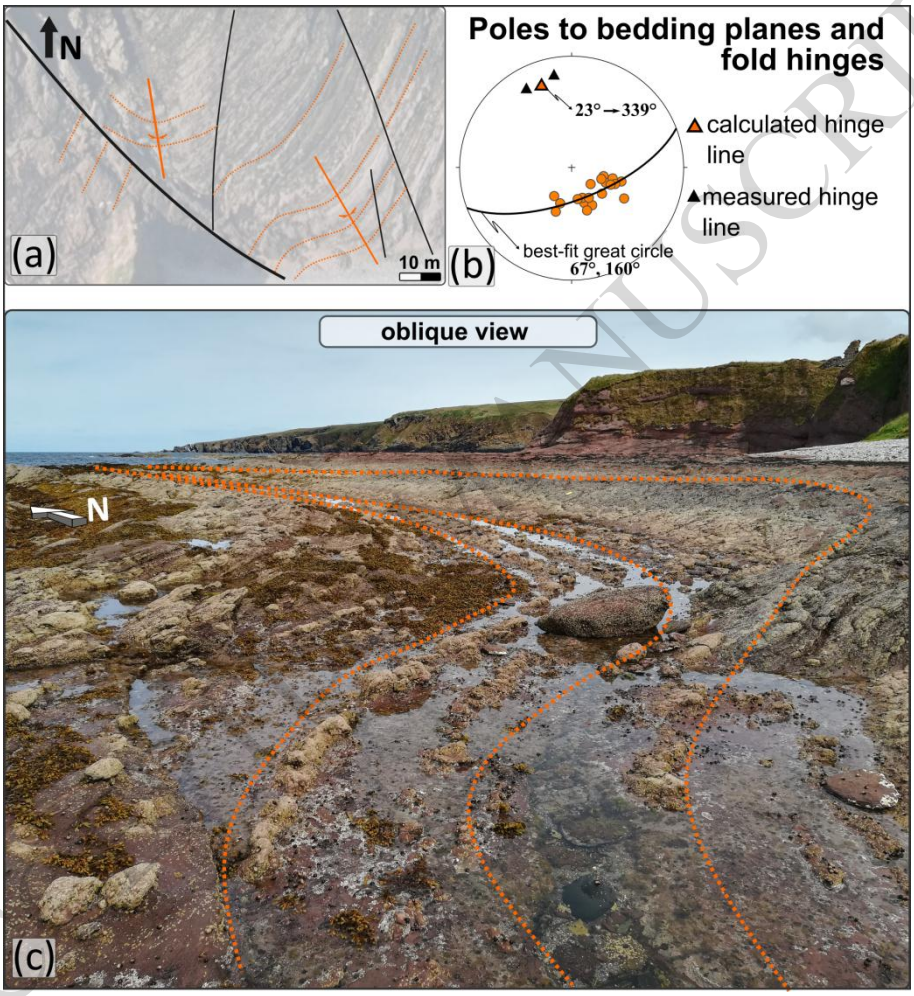

Figure 13

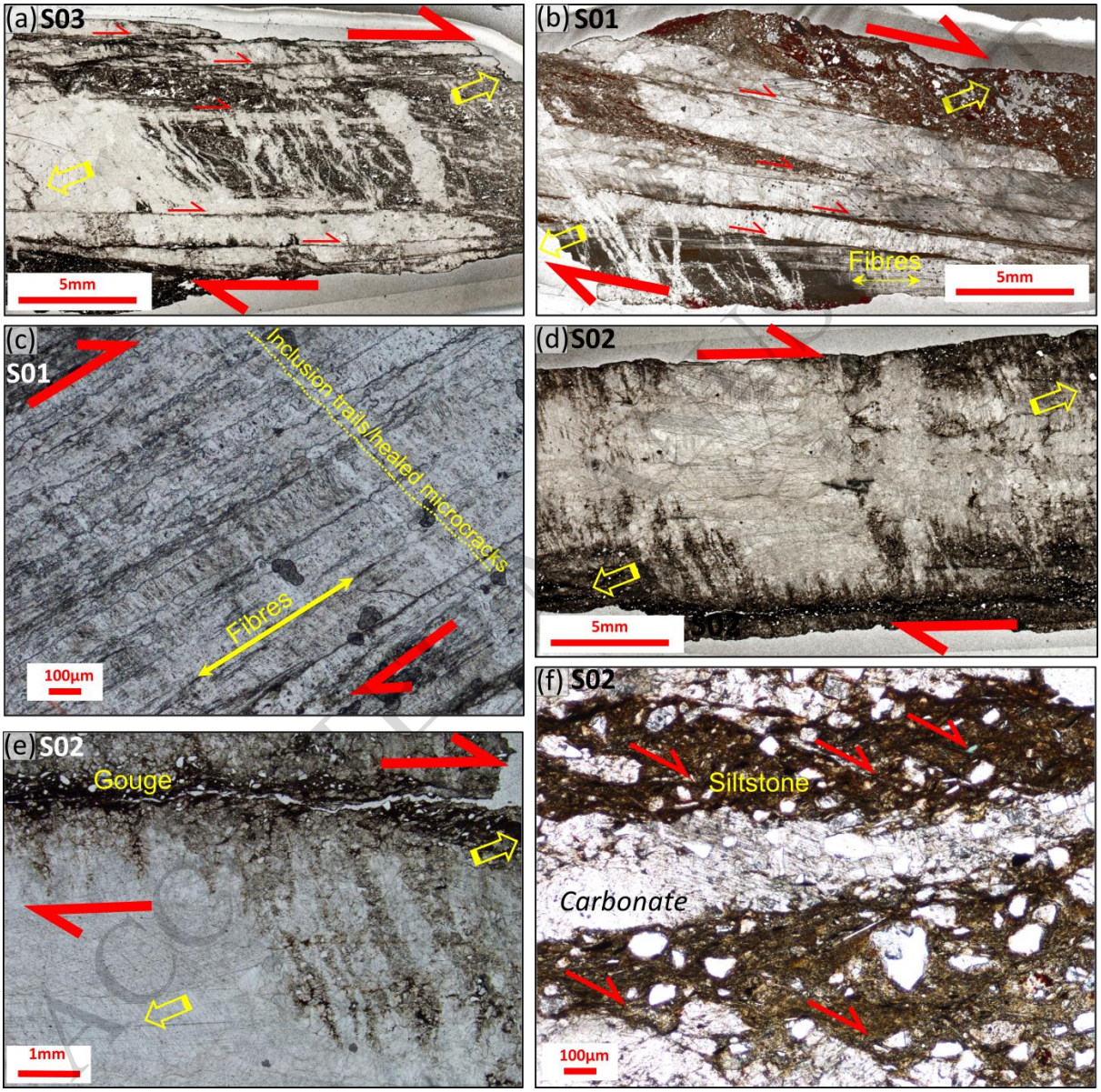

Figure 14

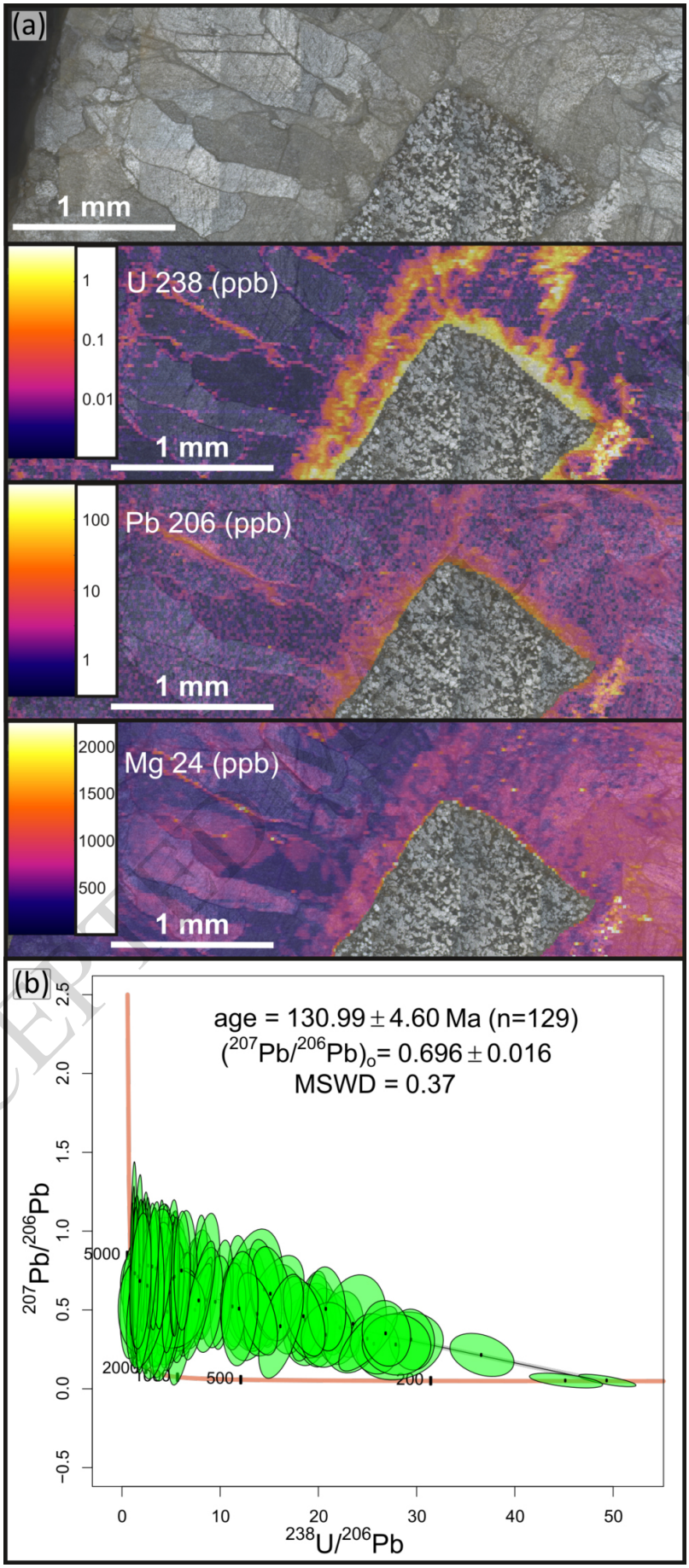

Figure 15

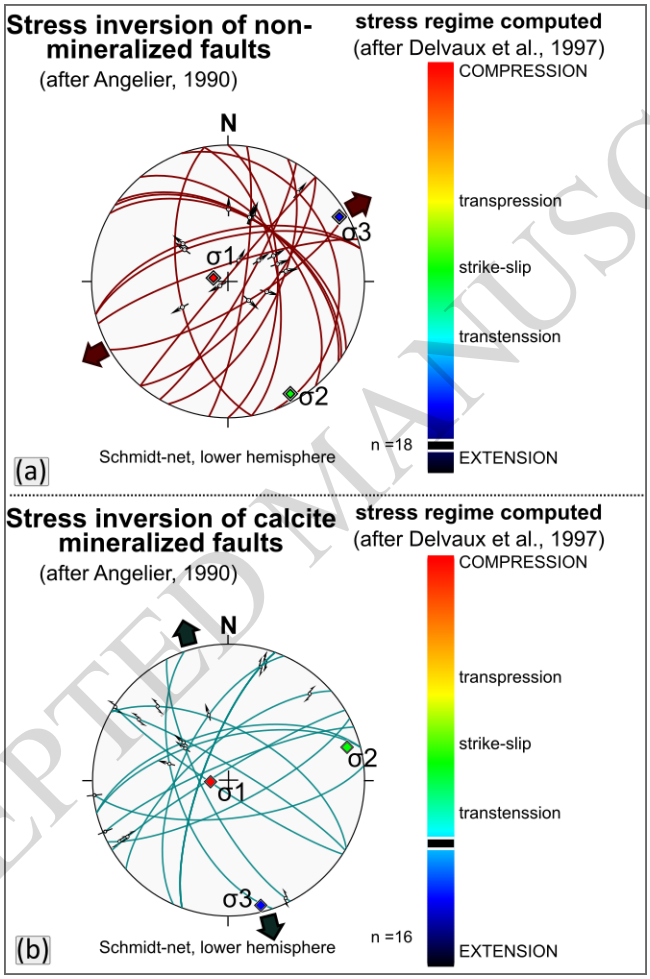

Figure 16